HHS Public Access

Author manuscript

Immunity. Author manuscript; available in PMC 2024 August 08.

Published in final edited form as:

Immunity. 2023 August 08; 56(8): 1894–1909.e5. doi:10.1016/j.immuni.2023.06.008.

Site-specific development and progressive maturation of human tissue resident memory T cells over infancy and childhood

Thomas J. Connors[1], **Rei Matsumoto**[2,3], **Shivali Verma**[2], **Peter A. Szabo**[2], **Rebecca Guyer**[2], **Joshua Gray**[2], **Zicheng Wang**[4], **Puspa Thapa**[2], **Pranay Dogra**[2], **Maya M.L. Poon**[2], **Ksenia Rybkina**[2], **Marissa C. Bradley**[1], **Emma Idzikowski**[1], **James McNichols**[5], **Masaru Kubota**[2,3], **Kalpana Pethe**[1], **Yufeng Shen**[4], **Mark A. Atkinson**[5], **Maigan Brusko**[5], **Todd M. Brusko**[5], **Andrew J. Yates**[6], **Peter A. Sims**[4,7], **Donna L. Farber**[2,3,*]

[1]Department of Pediatrics, Columbia University Vagelos College of Physicians and Surgeons, New York, NY 10032 USA

[2]Department of Microbiology and Immunology, Columbia University Irving Medical Center, New York, NY 10032 USA

[3]Department of Surgery, Columbia University Irving Medical Center, New York, NY 10032 USA

[4]Department of Systems Biology, Columbia University Irving Medical Center, New York, NY 10032 USA

[5]Department of Pathology, Immunology, and Laboratory Medicine, University of Florida, Gainesville, FL 32611, USA

[6]Department of Pathology and Cell Biology, Columbia University Irving Medical Center, New York, NY 10032 USA

[7]Department of Biochemistry and Molecular Biophysics, Columbia University Irving Medical Center, New York, NY 10032

SUMMARY

Infancy and childhood are critical life stages for generating immune memory to protect against pathogens; however, the timing, location, and pathways for memory development in humans remain elusive. Here, we investigated T cells in mucosal sites, lymphoid tissues, and blood from 96 pediatric donors aged 0–10 years using phenotypic, functional, and transcriptomic

*Lead Contact: df2396@cumc.columbia.edu.

Author Contributions

Conceptualization: TJC, DLF. Data Curation: TJC, SV. Formal Analysis: TJC, RM, SV, ZW, YS, AJY. Funding acquisition: TMB, DLF. Investigation: TJC, RM, SV, PASz, RG, PT, PD, MMLP, JG, KR, MCB, EI, JM, MK, KP, MAA, MB, TMB. Methodology: TJC, AJY, SV, YS, DLF. Project administration: DLF. Supervision: DLF. Visualization: TJC, RM, SV, ZW, YS, AJY. Writing – original draft: TJC, PASz, AJY, PASi, DLF. Writing – review & editing: all authors.

Declaration of Interests: The authors declare no competing interests.

Supplementary Excel Tables

Table S3. Related to Figure 5. RNA sequencing DE gene lists.

profiling. Our results revealed that memory T cells preferentially localized in intestines and lungs during infancy and accumulated more rapidly in mucosal sites compared to blood and lymphoid organs, consistent with site-specific antigen exposure. Early life mucosal memory T cells exhibit distinct functional capacities and stem-like transcriptional profiles. In later childhood, they progressively adopt pro-inflammatory functions and tissue resident signatures, coincident with increased TCR clonal expansion in mucosal and lymphoid sites. Together, our findings identify staged development of memory T cells targeted to tissues during the formative years, informing how we might promote and monitor immunity in children.

Graphical Abstract

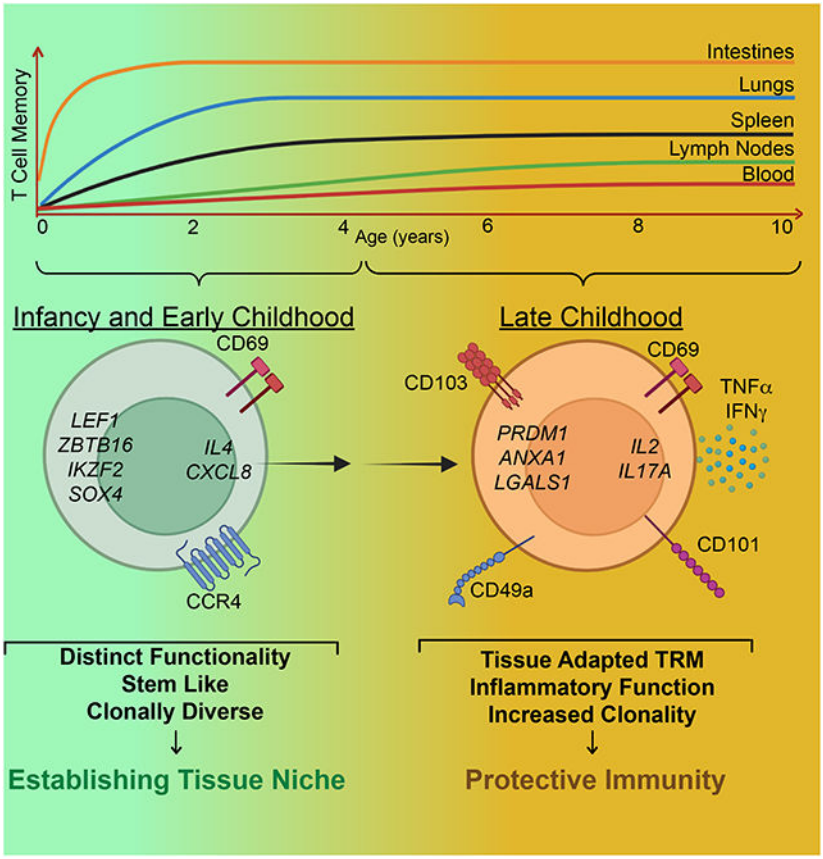

Immune memory generation during early childhood is critical for long-term protective immunity. Connors et al. analyze the development of human memory T cells in lymphoid organs, mucosal sites and blood over infancy and childhood. Memory T cells accumulate rapidly in intestines and lungs, and display age- and tissue-driven maturation stages.

Keywords

T cells; Infant Immunity; tissue resident memory T cells; mucosal immunity; developmental immunity

INTRODUCTION

Infancy and childhood are critical periods for development and maturation of adaptive immunity. During this time, the immune system establishes protective immunity to pathogens and tolerance to innocuous microbial and environmental antigens. T cell-mediated responses during this window can set the stage for a lifetime of protection and health or predispose to dysregulated immune responses including allergies and inflammatory diseases[1,2]. While it is well known that infection and vaccination during infancy and childhood can generate immune memory and lifelong protective immunity[3], identifying the pathways for T cell memory development during this life stage in humans has been elusive due to sampling constraints across all pediatric ages. A comprehensive understanding of human T cell differentiation and memory formation at the earliest life stages and defining when pediatric memory T cells reach functional maturation is needed to develop strategies for immune monitoring, vaccination, and immunotherapies targeted to children.

Immune memory is generated following primary responses to newly encountered antigens, which constitutes the majority of early life exposures. Naïve T cells are primed by antigen-bearing dendritic cells in lymphoid organs and subsequently differentiate to cytokine-producing effector cells. These effector cells migrate to sites of infection, and ultimately give rise to a heterogeneous memory pool maintained in blood and peripheral tissues. Tissue-resident memory T (T_{RM}) cells are generated in sites of prior antigenic exposure, predominate in mucosal and barrier sites, and are critical for coordinating rapid protective responses in mouse infection models[4–6]. In humans, T_{RM} cells are distinguished by a core phenotypic, functional, and transcriptional signature[7,8] and comprise the majority of T cells in mucosal and peripheral tissues of adults[7,9–11]. We found that the proportion of T_{RM} cells in specific sites, including the lungs and intestine remains stable over adulthood[7,9,12,13], suggesting that the dynamic events in T_{RM} formation occur much earlier in life.

The immune response in children is distinct from that of adults, and there are documented differences in activation and differentiation properties of neonatal compared to adult T cells[14]. In mouse models of virus infection, infant T cells exhibit higher proliferative responses and lower activation threshholds compared to adult T cells, and readily home to tissue sites of infection[14–17]. Despite the ability of early life T cells to generate tissue-homing, virus-specific effector cells, the subsequent development of memory T cells, including T_{RM} cells, is reduced in mice infected as infants compared to adults[14,17–19].

In humans, T cells respond to numerous pathogens which enter barrier and mucosal sites early after birth, as babies born without T cells (as in complete DiGeorge syndrome) develop multiple life-threatening infections at mucosal sites and succumb before 2yrs of age unless they receive a thymus transplant[20,21]. In blood, there is evidence for dynamic immune responses during the first weeks and months of life, though T cells remain predominantly naïve[22,23], suggesting T cell activation is occurring elsewhere. We and others have detected memory T cells in intestines during infancy[12,24–26]; however, the fate and functions of these early memory cells remain unknown, including whether T_{RM} cells develop directly from early exposures or require additional maturation. The pathways and timing for generation of functionally protective memory responses in humans have not yet been elucidated.

In this study, we analyzed samples obtained from 96 pediatric organ donors and study participants aged 0–10 years to reveal how T cell memory develops in mucosal sites and lymphoid organs and is manifested in blood from birth through the first decade of life. We identify site-specific accumulation of memory T cells in different sites, including rapid accrual of memory T cells in lungs and intestines during the first 3 years of life, and more gradual appearance of T cell memory in lymphoid organs and blood. We found that memory T cells exhibit staged maturation over childhood in mucosal sites coincident with downregulation of stem-like transcription factors; early mucosal memory T cells lack proinflammatory function and have reduced T_{RM} cell marker expression compared to mucosal memory T cells in children 4 years of age and older which exhibit mature T_{RM} phenotypes and function. Tracking TCR clonal dynamics reveals progressive increases in clonality over childhood in lymph nodes, consistent with dynamic priming of memory T cells at all ages. Our results identify key milestones in the development of T cell memory involving rapid mobilization in mucosal sites of high antigenic exposure and age-associated acquisition of tissue residency and functional capacity, leading to regional specialization of memory for robust protective immunity.

RESULTS

Pediatric samples to define immune development in blood and tissues

Pediatric blood and tissue samples including lungs, intestines, and lymphoid organs (spleen, lung- and gut-associated lymph nodes (LN)) were obtained from 68 organ donors, aged 0–10 years, including 30 donors <2 years of age to closely investigate this dynamic period of life (Figure 1A, Table S1; see Materials and Methods). Additional pediatric blood samples were obtained from children undergoing phlebotomy in the outpatient setting (aged 2 months-10 years (median age 2 years), n=28; Figure1A), including 12 subjects <2 years old. These pediatric cohorts represented a diverse racial and ethnic composition (Figure 1B). We analyzed these samples using confocal imaging, flow cytometry, and whole transcriptome profiling by RNA-sequencing (RNAseq) to determine how T cells populate tissues and develop immune memory over infancy and childhood, compared to adult tissues (n=8, Table S1).

Accumulation of αβ T cells in mucosal sites during early life

The extent to which T cells seed mucosal sites during early life was investigated by confocal imaging of lungs and intestines. Quantitative immunofluorescence (IF) analysis revealed low densities of conventional αβ T cells and γδ T cells (lymphocytes of restricted diversity which develop early in ontogeny[27]) in each site in the early weeks of life (Figure 1C, Figure S1A,B). During the first 3 years of life, there were marked increases in the densities of αβ T cells in both lungs and intestines, accumulating around airways and in the lamina propria, respectively (Figure 1D). While the jejunum exhibited a greater density of αβ T cells than the lungs (Figure S1C), the kinetics of accumulation were similar for each site with midpoints of their accumulation at ages 1.3 and 1.4 years, respectively (Figure 1D). By contrast, the density of γδ T cells remained constant in the lungs and declined slightly but significantly in the jejunum during the early years of life (Figure 1D, Figure S1C). By flow cytometry, we found decreased frequencies of γδ T cells over childhood in the

jejunum, consistent with imaging, and low frequencies of γδ T cells in the LN over age (Figure S2 and S3A). This progressive increase in αβ but not γδ T cells, in mucosal sites over the first few years of life suggest antigen-driven mechanisms rather than an autonomous developmental program.

Site-specific localization and accumulation of memory T cells over childhood

We hypothesized that the rapid increase in αβ T cells in mucosal sites was due to antigen-driven generation of effector and memory T cells. We used CD45RA and CCR7 expression to delineate naïve and previously activated or memory subsets including effector-memory (T_{EM}), central-memory (T_{CM}), and terminal effector (T_{EMRA}) cells[28] in blood and tissues of pediatric donors (Figure S2, S4). For assessing naïve and memory $CD4^+$ T cells, we excluded regulatory T cells (Treg cells, $CD4^+/CD127^-/CD25^+/FoxP3^+$) which are thymically derived; Treg cell frequencies were generally low in tissues (<10%) and declined after the early years of life in intestinal sites and associated LN (Figure S3B) consistent with prior studies[24]. Overall, naïve $CD4^+$ and $CD8^+$ T cells were the predominant αβ T cell subsets in lymphoid organs and lungs during the first year of life, while $CD4^+$ and $CD8^+$ T_{EM} (and CD8 T_{EMRA}) cells were present in intestinal sites even at birth (Figure 2A, Figure S4A). From ages 2–10 years, $CD4^+$ and $CD8^+$ T_{EM} cells were predominant in the intestines and lungs and exhibited substantial frequencies in lymphoid organs (Figure 2A). Across all ages, T_{CM} cells were more prevalent among $CD4^+$ compared to $CD8^+$ T cells, found in low frequencies in blood, lymphoid sites, and colon, while T_{EMRA} cells were mostly found among $CD8^+$ T cells in lung, spleen, and intestines (Figure 2A, Figure S4B). Comparing the frequencies of non-naïve subsets across sites revealed significant differences between mucosal and blood/lymphoid sites for T_{EM}, between gut and other sites for $CD4^+$ T_{CM}, and between spleen/lung and other sites for T_{EMRA} (Figure S4C). Together, these findings show compartmentalization of memory subsets during early life and childhood largely in mucosal sites.

To depict memory T cell accumulation more clearly in each site over age, we plotted the increase in total memory T cells ($T_{EM}+T_{CM}+T_{EMRA}$) and concomitant decrease in frequency of naïve T cells over age (Figure 2B). There was an exponential increase in memory accumulation in mucosal sites (lungs, small and large intestines) compared to more gradual, linear increases in blood and lymphoid organs (Figure 2B, Figure S5). For mucosal sites, the frequency of memory T cells approached 100% during the first 10 years, in contrast to lower magnitudes in lymphoid organs (25–60% in LN), and blood (~50%) (Figure 2B). These findings establish that the rate and magnitude of memory T cell accumulation is site-specific and markedly different between mucosal versus lymphoid sites. Moreover, T cell-based readouts of rapid memory formation during infancy are manifested in tissues and not in blood.

To define the kinetics of memory T cell prevalence more precisely, we characterized them empirically with logit-linear and non-linear models (Figure 2C). In mucosal sites, memory T cells accumulated rapidly, doubling their frequency each year in small intestines and achieving comparably high rates in lungs and colon (Figure 2C); the age at the midpoint of their accumulation was <6 months in jejunum and ileum, and approximately 1 year in lungs

and colon (Figure 2C). In stark contrast, the increase in memory T cell frequency in blood, LN, and spleen increased with age much more gradually--at <10% per year (Figure 2C). Together, these analyses reveal that site and timing are critical factors for memory T cell generation and naïve T cell maintenance.

Functional maturation of memory T cells is age and site-specific

A functional hallmark of memory T cells is their capacity to rapidly secrete different types of effector cytokines post-stimulation, known as rapid recall. To assess the intrinsic functional capacity of T_{EM} cells, we used short-term stimulation with PMA/ionomycin in the presence of protein secretion inhibitors to bypass TCR signaling and directly assess the cytokine production within cells. Our results revealed differences in the production of key pro-inflammatory cytokines, interferon-γ (IFN-γ) and/or tumor necrosis factor-α (TNF-α) between lineages, sites, and across age (Figure 3A). Between lineages, $CD4^+$ T_{EM} exhibited higher frequencies of TNF-α production compared to $CD8^+$ T_{EM} in spleen, lung, and intestines while $CD8^+$ T_{EM} produced more IFN-γ compared to $CD4^+$ T_{EM} in all sites examined (Figure 3A,B; Figure S6A). Between sites, T_{EM} in jejunum contained the highest frequencies of cytokine producers across all ages including putative multifunctional T_{EM} producing both IFN-γ and TNF-α (Figure 3B)— a feature of mature memory T cells in humans[29]. These findings demonstrate tissue-specific differences in functional capacity of memory T cells in children.

Across age, we identified progressive changes in memory T cell effector function in all sites. Memory T cells generated during infancy exhibited the lowest capacity for cytokine production compared to memory T cells isolated from older children (Figure 3A,C). There were increased proportions of $CD4^+$ and $CD8^+$ T_{EM} cells producing either IFN-γ or TNF-α or both throughout childhood and in all tissues, except the LLN which demonstrated similar trends but did not reach statistical significance (Figure 3C). Between sites, the pattern of functional maturation with age followed exponential kinetics in intestines and lungs and linear kinetics in blood and lymphoid organs (Figure 3C), similar to the pattern of overall memory accumulation. These results reveal three important aspects of pediatric memory T cells in humans: 1. Early life memory T cells are functionally hyporesponsive independent of site; 2. Memory T cells functionally mature over childhood; and 3. The magnitude and kinetics of memory T cell functional maturation is site-specific.

Progressive acquisition of tissue residency markers over childhood

The majority of $CD4^+$ and $CD8^+$ memory T cells in lymphoid and mucosal tissues at all pediatric ages expressed the canonical T_{RM} marker CD69, including 80–100% of mucosal memory T cells and 40–80% of lymphoid memory T cells (Figure 4A, Figure S6B). As expected, blood T cells lacked CD69 expression (Figure S6C). While there were slight but significant increases in CD69 expression with age over childhood in the spleen and LNs, (Figure 4A, Figure S6D), the high frequency of $CD69^+$ memory T cells in lungs and intestines was similar in magnitude for these same sites in adults[7,13]. Moreover, CD69 expression by pediatric memory T cells in tissues was not associated with activation markers including CD25, and cytokine production in the absence of stimulation (Figure S2, Figure 3). Together, these results indicate that CD69 expression by mucosal memory T cells is a

feature of localization in tissues and is not age-dependent; even at birth, memory T cells in all tissues express a core phenotypic marker of T_{RM} cells that distinguishes them from memory T cells in blood.

Expression of additional core T_{RM} cell markers[7], including the epithelial- and collagen-binding integrins CD103 and CD49a, respectively, the chemokine receptor CXCR6, and the negative regulator CD101[30] showed differential expression across sites and over age (Figure 4B,C; Figure S6B). For a several T_{RM} cell markers, the levels of expression by mucosal memory T cells in the early years of life was lower than observed in later childhood (Figure 4B, C). In particular, age-associated increases in CD103 surface expression were identified for lung $CD4^+$ T_{RM} and jejunum $CD8^+$ T_{RM} cells, CD101 expression for $CD4^+$ and $CD8^+$ T_{RM} cells in the lung and jejunum, and CXCR6 and CD49a expression for $CD4^+$ T_{RM} cells in the jejunum and lungs, respectively (Figure 4C). These results provide evidence for dynamic maturation and tissue adaptation of pediatric T_{RM} during the first decade of human life.

Transcriptional profiling reveals distinct stages of T_{RM} cell development

To elucidate the underlying mechanisms for developmental maturation of early life mucosal memory T cells we assessed their gene expression profile across infancy and childhood. We performed population-level RNA-seq of sorted $CD4^+CD69^+$ and $CD8^+CD69^+$ T_{EM} (T_{RM} phenotype, Figure S2) cells from lungs and intestinal sites (jejunum, ileum) and their associated LN of 11 pediatric organ donors aged 3 months – 8 years binned into 4 different age groups: 0–1yrs; 1–3yrs; 4–6yrs, and >7years (Table S2). This strategy enabled direct comparison of transcriptional properties of memory T cells having a T_{RM}-like phenotype across different ages. Principal component (PC) analysis of the transcriptional profiles for $CD8^+T_{RM}$ cells in mucosal tissue showed that samples separated based on tissue (PC1) and age (PC2) with the youngest donors (<3 years) grouped together and distinct from older donors (>4 years) (Figure 5A). The number of differentially expressed genes (DEG) for $CD8^+T_{RM}$ cells increased by age; there were low numbers of DEG between $CD8^+T_{RM}$ cells in infants and $CD8^+T_{RM}$ cells from 1–3 years in both sites, while there was a sharp increase in DEG relative to infant T_{RM} cells in the 4–6yr and 7–10yr groups (Figure 5B). Moreover, the number of DEG between infants and older children was higher in the intestines compared to lungs (Figure 5B), consistent with the increased magnitude and kinetics of changes in intestinal T cells during early childhood shown earlier. Similar age-associated clustering and increases in DEG was observed for $CD4^+T_{RM}$ cells in lungs and intestines (Figure S7A, B).

Pathway analysis revealed that the genes influencing changes with age for $CD8^+T_{RM}$ cells in the intestine (jejunum/ileum) and the lung were enriched for those regulating cellular differentiation, intracellular signal transduction, response to inflammation and cellular adhesion (Table S3). The specific genes which were significantly differentially expressed over age for T_{RM} cells in lungs and intestines are depicted in heat maps (Figure 5C). For both sites, there was a set of genes which were more highly expressed in the youngest donors, <3 years of age, and another set of genes that was significantly elevated in the older children >4 years of age (Figure 5C). The genes with increased expression in T_{RM}

cells from the youngest donors (0–3 years of age) included fate-determining transcription factors involved or implicated in T cell development: *IKZ2F* (Helios)[31], *ZBTB16* (PLZF)[32], *SOX4*[33,34], *ID3*[35]. Early T_{RM} cells also increased expression of the transcription factor *LEF1*, associated with stem-like properties[36].

Conversely, genes specifically elevated in lung and intestinal T_{RM} cells from older (>4 years) compared to the youngest children included multiple T_{RM} signature genes (*ITGA1* (CD49a), *CD101*, *ITGAE* (CD103), *CXCR6)*, *PRDM1,* a central regulator of T_{RM} cell formation in mice[37], and genes associated with tissue adaptation (*LGALS1*, *ANXA1*)[8]. We also found increased expression of site-specific genes in T_{RM} cells from older children including *CCR9* in intestinal T_{RM} cells, encoding a gut-homing marker[38] and *CTLA4* in lung T_{RM} cells, a negative regulator known to be elevated in adult lung T_{RM} cells[7](Figure 6C). There was also increased expression of genes encoding multiple effector cytokines, such as *IFNG*, *IL17A*, and *IL2,* in T_{RM} cells from older compared to the youngest donors within the lung (Figure 5C). Analysis of the gene expression for $CD4^+$ T_{RM} cells revealed similar age-related gene expression patterns with *IKZF2, SOX4,* and *LEF1* expressed by early life T_{RM} cells and *LGALS1*, *PRDM1*, *CD101*, expressed by T_{RM} cells from older children (Figure S7). These results demonstrate a marked shift in the transcriptional profile of early life memory T cells from a stem-like cell state lacking signatures for certain effector functions and tissue residence, to a fully differentiated T_{RM} cell expressing genes for core signature molecules, tissue adaptation, and effector function. These transcriptional results are also consistent with progressive increased expression of T_{RM} cell surface phenotypes and cytokine production shown above.

Distinct cytokine capacity of memory $CD4^+$ T cells in early compared to late childhood

Given the heterogeneity of $CD4^+$ T cell effector functions[39], we further interrogated changes in cytokine gene expression across age for mucosal memory $CD4^+$ T cells using the RNAseq dataset (Figure 6A). Across both lung and intestinal sites, $CD4^+$ T cells demonstrated age related changes in cytokine expression. In the intestine, transcripts encoding multiple cytokines associated with T_H2 cell responses (*IL4, IL5, and IL13)* and the chemokine IL8 (*CXCL8*), which recruits and activates neutrophils, were highest in memory $CD4^+$ T cells from the youngest donors (0–3yrs of age) and decreased in older children >4 years of age (Figure 6A). These results in intestines are consistent with previous studies showing predominant Th2 responses in neonatal mice[40,41] and IL-8 was produced by newborn human T cells[42]; however, we did not see similar age-associated trends for Th2 and IL-8 genes in lung memory $CD4^+$ T cells (Figure 6A). Over childhood, lung memory $CD4^+$ T cells exhibited increased expression of transcripts encoding TNF-α (Figure 6A), consistent with cytokine secretion assays (Figure 3).

To further validate the functional state of mucosal memory $CD4^+$ T cells, we assessed the surface expression of chemokine receptors associated with major T-helper cell lineages including CXCR3 for Th1 cells, CCR4 for Th2 cells, and CCR6 for Th17 cells[43,44]. Expression of CCR4 denoting Th2-like cells was higher in the intestine of donors <2 years of age compared to donors >4 years old and was also increased in lung CD4 T cells of younger compared to older children (Figure 6B). Expression of CXCR3 and CCR6

showed greater variation in intestinal compared to lung $CD4^+$ T cells but was not different between age groups. Together, these findings point to a shift in the functional profile of mucosal memory $CD4^+$ T cells in early years of life as being skewed to production of Th2-like cytokines and certain inflammatory mediators compared to memory $CD4^+$ T cells in children >4yrs of age which exhibit mature Th1-like profiles and variable IL-17 production depending on site. These functional distinctions for memory $CD4^+$ T cells are more strikingly manifested in the intestine, though they are more functionally heterogeneous across sites and donors than for memory $CD8^+$ T cells.

Dynamic shifts in clonal diversity and tissue compartmentalization over childhood

Antigen exposure results in clonal expansion of T cells. To examine whether memory formation at different ages is associated with expansion of specific clones within or across tissues, we investigated the TCR repertoire including clonal expansion, distribution, and overlap across sites. We applied MiXCR to our population RNA-seq dataset, which included data from lung- and gut-associated LN (Table S5) (Figure 7A). Across sites and donors, $CD8^+$ T_{RM} cells were more clonally expanded than $CD4^+$ T_{RM} cells, and T cells in mucosal sites were more expanded compared to LN (Figure 7A). These trends are similar to our previous TCR repertoire analysis of memory T cells in adult tissues[45].

To characterize the extent of clonal expansion across tissue sites and age, we calculated R20 and R50, which denotes the fraction of total clones which cumulatively account for 20% and 50%, respectively of the sequenced repertoire (Figure 7B). R20 and R50 were similar (5–10%) across sites in the youngest donors, indicating a polyclonal memory response, but decreased over age rapidly in mucosal sites following exponential kinetics, and more gradually in lymphoid sites. This decrease in frequency occupied by R20 and R50 indicates clonal expansion over age, consistent with antigen-driven activation. We then assessed how the clonal repertoire was shared across tissue sites within individual donors (Figure 7C). Clonal overlap between sites was minimal in the youngest donors (<2 years of age); however, after 2 years of age, overlap between certain tissues was evident and increased with age (Figure 7C). Across all donors, the highest overlap was observed between adjacent mucosal sites (jejunum-ileum) followed by clonal overlap between mucosal sites and corresponding LNs (jejunum-GLN, ileum-GLN), which also increased with age. (Figure 7D). Across all ages, however, overlap was negligible between intestinal and lung sites (Figure 7D), suggesting compartmentalization of clonal repertoires. These results provide evidence that early life memory T cells comprise expanded and tissue-segregated clones, which become more expanded, and migrate between adjacent sites over childhood.

DISCUSSION

Our study provides a high-dimensional analysis of T cell development and memory formation during the critical developmental window of early life and childhood in multiple tissues and blood. We reveal rapid generation of memory T cells targeted specifically to mucosal sites, with slower accumulation in lymphoid sites and blood. Mucosal memory T cells in early life exhibit low effector function and expression of tissue residence markers, but progressively mature over childhood to resemble functional, tissue adapted T_{RM} cells

by the end of the first decade of life. We further establish that T_{RM} cells generated in the early years of life comprise a distinct and transcriptional state expressing stem-like transcription factors, suggesting a role in establishing a memory cell niche for maturation of functionally protective T_{RM} cells that predominate later in childhood. Finally, we reveal that seeding of clonally related memory T cells across distinct tissue environments occurs progressively over the course of childhood. These results establish the timing, localization, and developmental pathways promoting regional specialization of immune memory.

It is well-established in mouse models that tissue-localized T_{RM} cells are important for protective immunity at sites of pathogen exposure[6,46,47]. In mice, one can track and analyze the primary response to a new pathogen and the subsequent development of memory in a completely naïve host. In humans, pathogen exposure in naïve hosts occurs mainly during early life and childhood, yet little is known about memory generation during this critical life stage. Here, we present a comprehensive analysis of memory T cell development across blood, multiple lymphoid organs, and key mucosal sites (lungs and intestines) obtained from infant and pediatric donors spanning birth through 10 years of age. We reveal that memory T cells are found predominantly in mucosal sites during the early years of life and exhibit rapid and exponential accumulation in the first 1–3 years both by frequency and absolute number. This biased accumulation of memory T cells in mucosal sites correlates with continuous exposure to a plethora of new antigens through breathing, eating, and the environment, and the known protective requirement of T cells in response to respiratory and enteric pathogens[21,48]. In mouse models, memory phenotype T cells can also be generated by lymphopenia-induced proliferation; transfer of naïve T cells into lymphocyte-deficient mice results in conversion to a memory phenotype driven by self-antigens, microbiome, and/or cytokines[49–51]. In humans, the rapid accrual of mucosal memory T cells over the first 2–3 years suggests that multiple types of antigens and factors may be involved.

Here, we identify that development of human T_{RM} cells in mucosal sites occurs in discrete stages. Mucosal memory T cells generated during the first 3 years are distinct from those detected in later childhood in their reduced ability to produce multiple proinflammatory cytokines such as IFN-γ and TNF-α, and their reduced expression of T_{RM} markers. However, these early mucosal memory T cells still exhibit the core features of antigen-experienced cells including expression of tissue memory phenotypes ($CD45RO^+CCR7^-CD69^+$), upregulation of effector cytokine genes that are known to be associated with infant responses (i.e., IL-8, IL-4, and IL-13)[42], and clonal expansions that increase with age. These early mucosal memory T cells could play roles in establishing the tissue niche and tolerance to mucosal exposures. Our results show that the Th2 bias is enhanced in intestines and may play a role in tolerance to food antigens that is known to occur in humans through early life exposures[52]. The second stage of T_{RM} development is manifested after 3–4 years of age and marked by a functional shift to proinflammatory cytokine production including IFN-γ, reduced Th2 responses, and an increase in expression of T_{RM} and tissue adaptation markers. These pediatric T_{RM} cells resemble functionally protective T_{RM} cells in mice and mature T_{RM} cells in human tissues[6,7,37,53].

The exact mechanisms for this staged maturation of human memory T cells over infancy and childhood are not clear; however, antigenic exposures and the tissue environment are

likely contributing factors. Repeat exposures to ubiquitous pathogens over childhood could promote functional differentiation of memory T cells. We previously showed that children exhibited lower frequencies of influenza-specific T cells and T_{RM} phenotypes in the lungs and LLN compared to adults[54], consistent with this phenomenon. The tissue environment itself including the microbiome that is known to undergo dynamic maturation in the first 3 years of life[55], and different cytokines and factors that result from the endogenous flora and developing tissue could also influence memory T cell maturation and phenotype. This maturation likely occurs *in situ* in mucosal sites, given our findings that lungs and jejunum retain clonal segregation of the TCR repertoire throughout childhood. In later childhood, priming in mucosal-associated lymph nodes and migration to the associated mucosal sites begins to establish local clonal neighborhoods, along with expansion of existing mucosal clones. This regional specialization of T cell memory is therefore established in the critical window of childhood.

Tissue compartmentalization of memory T cells at the earliest life stage as suggested by our findings has multiple implications for T_{RM} cell longevity and for site- and age-specific targeting of tissue responses. We have reported that T_{RM} cells in adult lungs and intestines express tissue-adapted phenotypes and transcriptional profiles and contain expanded clones that are segregated in each site[7,45,56,57], similar to what we find in childhood. These results suggest that T_{RM} cells generated during childhood may establish an early niche and persist long term. Moreover, the focused generation of memory in tissues during early life and the relative paucity of memory T cells in blood further suggests that blood may not be a reliable site for quantitative assessment of T cell responses during childhood. Conversely, site-directed strategies for promoting tissue-specific memory generation and immunity to vaccines may be particularly successful during the early years of life.

In summary, our results provide compelling evidence for tissue directed maturation of adaptive immunity during the formative years of early life and childhood to establish the landscape of immune protection and health for a lifetime.

Limitations of the Study

Because this is a study in humans and in samples obtained from deceased organ donors, it is not possible to assess the antigen specificity of the diverse population of memory T cells that are generated from the many different antigens encountered during early life and childhood. The low numbers of memory T cells present in mucosal sites during the first year of life also precludes direct testing for antigen-specific T cells by conventional peptide stimulation or tetramers using current technologies. Identifying the different types of stimuli, antigenic, microbiome, self-antigen, and cytokines involved in early memory T cell formation remains an avenue for further research. The direct role of specific transcription factors in the developmental shift from early life to mature T_{RM} cells in humans also requires additional studies.

STAR Methods

RESOURCE AVAILABILITY

Lead contact—Further information and requests for reagents should be directed to and will be fulfilled by the lead contact Donna L. Farber (df2396@cumc.columbia.edu)

Materials availability—This study did not generate new unique reagents.

Data and code availability—Population RNAseq data has been uploaded to GEO and are publicly available as of the date of publication. Accession number is listed in key resources table.

No original code was created for the purposes of this study.

Any additional information required to reanalyze the data reported in this paper is available from the lead contact upon request.

EXPERIMENTAL MODEL AND STUDY PARTICIPANT DETAILS

Human samples

Organ Donors: Tissues from deceased organ donors were obtained at time of organ acquisition for clinical transplantation from donors whose consent for use of tissues for research was obtained by next-of kin through collaborations and research protocols with organ procurement organizations (OPO). Tissues from pediatric organ donors were obtained through the Human Atlas for Neonatal DEveLopment (HANDEL) program based on the network for Pancreatic Organ Donors with Diabetes (nPOD) program[58] involving Material transfer agreements with OPOs throughout the USA. Tissues from adult organ donors were obtained through an approved and longstanding protocol and material transfer agreement with LiveOnNY, the OPO for the New York metropolitan area, as previously described[7,24,59,60]. Donors used in this study (see Table S1) were free of cancer, seronegative for hepatitis B, C, and HIV, and had no evidence of active infection based on respiratory, blood, and urine surveillance testing. The use of tissues from organ donors does not qualify as human subjects research as confirmed by the Columbia University IRB, as tissues are obtained from deceased, not living, individuals.

Outpatient Subjects: Informed consent was obtained from parents under a protocol approved by the Institutional Review Board of Columbia University Medical Center (New York, NY) to collect blood for research from children aged 0–10yrs having routine phlebotomy for clinical purposes. Subjects were seen across medical campus for routine pediatric care or elective surgical procedures.

METHOD DETAILS

Sample Processing—Organ donor samples (whole lungs, intestinal blocks, spleen, blood) in saline or University of Wisconsin solution were placed on ice, transported to the laboratory, and processed within 24–36 hours of procurement. Single cell suspensions were obtained from spleen, lungs, small and large intestines, and associated lymph nodes (LN)

using mechanical and enzymatic digestion as previously described[24,59,61]. Lymph nodes were isolated by dissection from the mesentery of intestinal blocks and the tracheobronchial tree of the lung. Isolated LN and spleen samples were placed in complete media (IMDM (Gibco, ref #12440-053) +1% PSQ (100 U/ml penicillin, 100 μg/ml streptomycin, 2 mM L-glutamine, GeminiBio, cat #c400-110) + 10% FBS (GeminiBio, cat #100-106)) and mechanically disrupted with scissors and double filtered through 100μm strainers. Suspensions were washed with wash buffer (PBS (Corning, cat #20-030-CV) + 2mM EDTA (Corning, cat #46-034-CI) + 5% FBS) followed by red blood cell lysis (ACK lysing buffer, Gibco, ref A10492-01), then resuspended in complete media. Lung parenchyma were separated from the large airways (trachea) using scissors then placed into digestion media (IMDM + Collagenase D 1mg/mL (Millipore Sigma cat# 11088882001) and + DNAse 0.1mg/mL (Millipore Sigma cat# DN25-5G) on a shaker at 37°Cfor 30 minutes. Intestinal tissue was washed with sterile PBS to remove luminal contents, chopped into pieces using scissors, then placed into digestion media on a shaker at 37°C for 30 minutes. Following incubation, lung and intestinal samples were strained and washed with wash buffer. Samples were centrifuged with resultant cell pellet diluted for mononuclear cells isolation by density gradient centrifugation (Lymphocyte Separation Medium, Corning, cat #25-072-CI) followed by resuspension in complete media. Peripheral blood mononuclear cells were isolated from blood samples by density centrifugation.

Immunofluorescence Imaging—Lung and intestinal tissue were cut into 0.5cm thickness samples and fixed with 4% paraformaldehyde, lysine and periodate buffer (PLP, 0.05 M phosphate buffer, 0.1 M L-lysine, pH 7.4, 2mg/mL $NaI0_4$, and 10mg/mL paraformaldehyde). Samples were then placed on a shaker and maintained at 4°C overnight. Samples were then washed with PLP buffer and placed into 30% sucrose solution for 48 hours at 4°C followed by embedding in OCT (Fisher Healthcare, cat#23-730-571) compound. Samples were then frozen and stored at −80°C. Frozen samples used for imaging were sectioned using a Leica CM1950 cryostat to 20μm thickness. Prior to antibody staining, Fc blocking was performed using human TruStain FcX (Biolegend, cat #422302) diluted in PBS (Corning, cat #20-030-CV) containing 2% goat serum and 5% FBS for 1 hour at room temperature (RT). Sections were then stained with DAPI and fluorescent tagged antibodies for 1 hour at RT protected from light. Images were acquired using a Nikon A1 confocal microscope. Imaged data were analyzed using Imaris software (Bitplane; Oxford Instruments) using surface creation and spot detection functions. Two sections per donor were imaged for intestinal sites with area and positive cells calculated per 1cm of tissue. Three sections per donor were imaged for lung tissue with area and positive cells calculated around 4–5 central airways per donor.

Flow cytometry and Cell Sorting—Single cell suspensions were stained with fluorescently labeled antibodies for flow cytometry analysis and sorting. For analytical flow cytometry, cells were washed with FACS buffer (PBS with 2% heat inactivated FBS) then resuspended in human TruStain FcX for 10 min at RT. For surface staining, fluorochrome-conjugated antibodies (STAR methods) in FACS buffer were added to cell suspensions for 20 minutes at RT protected from light, followed by washing with FACS-buffer, centrifugation, and resuspension in fixation buffer (Invitrogen, cat #00-5223-56

and #00-5123-43) for 20 minutes on ice. Following fixation, cells were washed with FACS buffer, and stained with antibodies for intracellular detection (STAR methods) in permeabilization buffer (Invitrogen, cat #00-8333-56) for 20 minutes on ice, followed by washing and resuspension in FACS buffer. Stained cells were analyzed using the BD LSRII or Cytek Aurora flow cytometer. For cell sorting, cells were washed with EasySep Buffer (PBS with 2% heat inactivated FBS and 1mM EDTA) then resuspended in TruStain FcX for 10 min at RT. Surface stain was added to cell suspension using fluorochrome-conjugated antibodies in FACS buffer for 20 minutes at RT protected from light, then washed in FACS buffer followed by centrifugation and resuspension in FACS buffer. Cell populations were sorted into FBS on an BD Influx Cell Sorter.

***Ex vivo* T cell stimulations—**Single cell mononuclear suspensions isolated from blood and tissue samples prepared as above were plated in 96 well U-bottom plates ($5X10^6$ cells per well) in 500μL of complete media (as described above) containing PMA (Sigma, Cat#P1585) (50ng/mL) plus ionomycin (Sigma, Cat#I9657) (1μg/mL). Stimulated cells were incubated at 37°C for 4 hours in the presence of GolgiStop (BD Biosciences, cat#554724) and GolgiPlug (BD Bioscience cat#555029). Cells were washed, stained with fixable viability marker (Zombie NIR, Biolegend, cat#423106) prior to surface and intracellular staining.

Whole transcriptome profiling by RNAseq—Tissue resident memory phenotype ($CD45RA^-CCR7^-CD69^+$) $CD4^+$ and $CD8^+$ T cells were sorted from lungs, jejunum, ileum, colon, and associated lymph nodes from organ donors aged 0.33–8 years of age (Table S2). Following sorting, samples (>10,000 cells) were centrifuged and resuspended in RLT Buffer Plus (Qiagen, cat #1053393) with β-mercaptoethanol (Sigma, cat #M6250-250ML) and stored at −80°C until RNA extraction. RNA extraction was done using the RNeasy Micro Kit (Qiagen, cat#74004) and the resultant RNA was resuspended in water and run on an Agilent Bioanalyzer using the RNA 6000 Pico Kit (Agilent, cat #5067-1513) to assess RNA integrity. Library preparation was done using the SMART-Seq® ultra-low input RNA kit (Takara bio). RNA samples were sequenced (2×150 paired end) at GENEWIZ (South Plainfield, NJ) using a HiSeq2500 system (Ilumina). Trimmed paired-end reads were aligned to the Homo sapiens GRCh38 reference genome available on ENSEMBL using the STAR aligner v.2.5.2b. Read quantification was done by Genewiz using featureCounts on the Subread package v.1.5.2. Differential gene expression analysis and principal component analysis was performed using DESeq2[62]. Visualization of differentially expressed genes between age groups was done using Venn diagrams[63], diffggplot2, and GraphPad Prism. Heatmaps were generated using the pheatmap[64] package. Geneset enrichment analysis was performed using GSEA software[65,66](ver 4.3.1; UC San Diego and Broad Institute) using a preranked gene list based on log2 fold change of differentially expressed genes between infant organ donors (<1 year) and oldest organ donors (>4 years) by tissue site.

Extraction and analysis of TCR repertoire from T cell RNA-seq data—The MiXCR analysis pipeline[67] was used to extract TCR repertoire data from the RNA-seq datasets described above. Using default parameters, sequencing reads within the fastq files were aligned against reference V,D,J, and C genes, followed by contig assembly and export

of all TCR clonotypes with associated clone counts. We used the *TRBV* CDR3 nucleotide sequence as a proxy of T cell clonal identity and was analyzed using metrics of diversity and clonal overlap. Repertoire diversity was quantified using the R20 score, which is defined by the fraction of unique clones, in descending order of frequency, which account for 20% of the sequenced repertoire[68]. Repertoire overlap between tissues was quantified as the ratio of intersection to union of total clonotypes from compared tissues. The correlation between ages and diversity/clonal overlap was analyzed using the linear least-squares regression function of SciPy[69].

QUANTIFICATION AND STATISTICAL ANALYSIS

Flow cytometry data were analyzed using FCS express (ver. 7.12.0005) and FlowJo (ver. 10.7.1). Descriptive analyses and statistical testing of compiled flow cytometry and imaging data were performed using Prism (GraphPad ver. 9.3.1) and *R*. To analyze the kinetics of memory T cell prevalence within the mucosal and lymphoid sites (Figure 2), percentages were converted to frequencies and then logit-transformed to normalize scatter across the range of measurements. For each memory T cell subset at each location we then fitted two descriptive models to the time course of its frequency, using least-squares approaches (the lm() and nls() functions in *R*). One model assumed a linear dependence of the transformed frequency (f) on age (t), $f(t) = f_0 + pt$. The other took a nonlinear (saturating exponential) form, $(t) = f_0 + (f_1 - f_0)(1 - e^{-rt})$, where f_0 and f_1 are the initial and endpoint values of the transformed memory T cell frequency, respectively, and the rate r reflects the steepness of the approach to the endpoint. We compared the fits of these non-nested models using the Akaike Information Criterion (AIC), with the simpler linear model favored for absolute differences in AIC smaller than 2. The trajectories of memory T cell frequencies in mucosal tissues were uniformly described best by the saturating exponential model (ΔAIC between 4 and 22 relative to the linear model). The linear model was favored for all subsets in all lymphoid sites, except for $CD4^+$ T cell memory in GLN (ΔAIC = 11 in favor of nonlinear). In that instance the fitted predictions were visually very close to linear in form and we selected the linear model for clarity. Prediction curves for all models were generated using the inverse logit-transform to map fitted values back to cell frequencies. For nonlinear fits, rates of accumulation of memory are quoted at the mid-point of the growth curve on the untransformed scale. For the log-linear fits we quote the average growth rates on the untransformed scale. 95% confidence intervals on all rate estimates and best-fit prediction curves were generated by bootstrapping (N=1999). The 95% confidence intervals on the estimated growth rates of memory $CD4^+$ and $CD8^+$ T cells in blood spanned zero but are truncated in Figure 3C due to the logarithmic scale.

Supplementary Material

Refer to Web version on PubMed Central for supplementary material.

Acknowledgements

We extend our gratitude to the families whose gift of organ donation made this work possible. We acknowledge the dedication and support of Mingder Yang and Robert O'Flynn from the network for Pancreatic Organ Donors with Diabetes (nPOD), the transplant coordinators and staff of LiveOnNY, Carlos Aguilar-Breton for human subject acquisition. This work was supported by the US National Institutes of Health (NIH) (Grant nos. AI106697,

AI100119, AI168634 to DLF; AI150650 to A.J.Y. and D.L.F.; AI106697 and AI128949 to P.A.S.; AI141686 to TJC), and the Helmsley Charitable trust to TMB and DLF. PASz was supported by a Canadian Institutes of Health Research Fellowship. Research reported here was performed in the Columbia Flow Cytometry Core (supported by NIH awards S10RR027050, S10OD020056), the Sulzberger Columbia Genome Center, and the Columbia Single Cell Analysis Core (supported by grant P30CA013696). Additional support was provided in part by Columbia University's CTSA grant No. UL1TR001873 from NCATS/NIH. The content is solely the responsibility of the authors and does not necessarily represent official views of the NIH.

Inclusion and Diversity

We support inclusive, diverse, and equitable conduct of research.

REFERENCES

1. Bach JF (2002). The effect of infections on susceptibility to autoimmune and allergic diseases. N Engl J Med 347, 911–920. 10.1056/NEJMra020100. [PubMed: 12239261]
2. Reynolds LA, and Finlay BB (2017). Early life factors that affect allergy development. Nat Rev Immunol 17, 518–528. 10.1038/nri.2017.39. [PubMed: 28504257]
3. Amanna IJ, Carlson NE, and Slifka MK (2007). Duration of humoral immunity to common viral and vaccine antigens. N Engl J Med 357, 1903–1915. 10.1056/NEJMoa066092. [PubMed: 17989383]
4. Szabo PA, Miron M, and Farber DL (2019). Location, location, location: Tissue resident memory T cells in mice and humans. Sci Immunol 4, eaas9673. 10.1126/sciimmunol.aas9673.
5. Masopust D, and Soerens AG (2019). Tissue-Resident T Cells and Other Resident Leukocytes. Annu Rev Immunol 37, 521–546. 10.1146/annurev-immunol-042617-053214. [PubMed: 30726153]
6. Paik DH, and Farber DL (2021). Anti-viral protective capacity of tissue resident memory T cells. Curr Opin Virol 46, 20–26. 10.1016/j.coviro.2020.09.006. [PubMed: 33130326]
7. Kumar BV, Ma W, Miron M, Granot T, Guyer RS, Carpenter DJ, Senda T, Sun X, Ho SH, Lerner H, et al. (2017). Human Tissue-Resident Memory T Cells Are Defined by Core Transcriptional and Functional Signatures in Lymphoid and Mucosal Sites. Cell Rep 20, 2921–2934. 10.1016/j.celrep.2017.08.078. [PubMed: 28930685]
8. Szabo PA, Levitin HM, Miron M, Snyder ME, Senda T, Yuan J, Cheng YL, Bush EC, Dogra P, Thapa P, et al. (2019). Single-cell transcriptomics of human T cells reveals tissue and activation signatures in health and disease. Nat Commun 10, 4706. 10.1038/s41467-019-12464-3. [PubMed: 31624246]
9. Kumar BV, Connors TJ, and Farber DL (2018). Human T Cell Development, Localization, and Function throughout Life. Immunity 48, 202–213. 10.1016/j.immuni.2018.01.007. [PubMed: 29466753]
10. Pallett LJ, Davies J, Colbeck EJ, Robertson F, Hansi N, Easom NJW, Burton AR, Stegmann KA, Schurich A, Swadling L, et al. (2017). IL-2(high) tissue-resident T cells in the human liver: Sentinels for hepatotropic infection. J Exp Med 214, 1567–1580. 10.1084/jem.20162115. [PubMed: 28526759]
11. Weisberg SP, Carpenter DJ, Chait M, Dogra P, Gartrell-Corrado RD, Chen AX, Campbell S, Liu W, Saraf P, Snyder ME, et al. (2019). Tissue-Resident Memory T Cells Mediate Immune Homeostasis in the Human Pancreas through the PD-1/PD-L1 Pathway. Cell Rep 29, 3916–3932 e3915. 10.1016/j.celrep.2019.11.056. [PubMed: 31851923]
12. Senda T, Dogra P, Granot T, Furuhashi K, Snyder ME, Carpenter DJ, Szabo PA, Thapa P, Miron M, and Farber DL (2019). Microanatomical dissection of human intestinal T-cell immunity reveals site-specific changes in gut-associated lymphoid tissues over life. Mucosal Immunol 12, 378–389. 10.1038/s41385-018-0110-8. [PubMed: 30523311]
13. Thome JJ, Yudanin N, Ohmura Y, Kubota M, Grinshpun B, Sathaliyawala T, Kato T, Lerner H, Shen Y, and Farber DL (2014). Spatial map of human T cell compartmentalization and maintenance over decades of life. Cell 159, 814–828. 10.1016/j.cell.2014.10.026. [PubMed: 25417158]
14. Rudd BD (2020). Neonatal T Cells: A Reinterpretation. Annu Rev Immunol 38, 229–247. 10.1146/annurev-immunol-091319-083608. [PubMed: 31928469]

15. Reynaldi A, Smith NL, Schlub TE, Venturi V, Rudd BD, and Davenport MP (2016). Modeling the dynamics of neonatal CD8(+) T-cell responses. Immunol Cell Biol 94, 838–848. 10.1038/icb.2016.47. [PubMed: 27142943]

16. Smith NL, Wissink E, Wang J, Pinello JF, Davenport MP, Grimson A, and Rudd BD (2014). Rapid proliferation and differentiation impairs the development of memory CD8+ T cells in early life. J Immunol 193, 177–184. 10.4049/jimmunol.1400553. [PubMed: 24850719]

17. Zens KD, Chen JK, Guyer RS, Wu FL, Cvetkovski F, Miron M, and Farber DL (2017). Reduced generation of lung tissue-resident memory T cells during infancy. J Exp Med 214, 2915–2932. 10.1084/jem.20170521. [PubMed: 28855242]

18. Zens KD, Connors T, and Farber DL (2017). Tissue compartmentalization of T cell responses during early life. Semin Immunopathol. 10.1007/s00281-017-0648-7.

19. Thapa P, Guyer RS, Yang AY, Parks CA, Brusko TM, Brusko M, Connors TJ, and Farber DL (2021). Infant T cells are developmentally adapted for robust lung immune responses through enhanced T cell receptor signaling. Sci Immunol 6, eabj0789. 10.1126/sciimmunol.abj0789.

20. Markert ML, Boeck A, Hale LP, Kloster AL, McLaughlin TM, Batchvarova MN, Douek DC, Koup RA, Kostyu DD, Ward FE, et al. (1999). Transplantation of thymus tissue in complete DiGeorge syndrome. N Engl J Med 341, 1180–1189. [PubMed: 10523153]

21. Markert ML, Sarzotti M, Ozaki DA, Sempowski GD, Rhein ME, Hale LP, Le Deist F, Alexieff MJ, Li J, Hauser ER, et al. (2003). Thymus transplantation in complete DiGeorge syndrome: immunologic and safety evaluations in 12 patients. Blood 102, 1121–1130. [PubMed: 12702512]

22. Olin A, Henckel E, Chen Y, Lakshmikanth T, Pou C, Mikes J, Gustafsson A, Bernhardsson AK, Zhang C, Bohlin K, and Brodin P (2018). Stereotypic Immune System Development in Newborn Children. Cell 174, 1277–1292 e1214. 10.1016/j.cell.2018.06.045. [PubMed: 30142345]

23. Lee AH, Shannon CP, Amenyogbe N, Bennike TB, Diray-Arce J, Idoko OT, Gill EE, Ben-Othman R, Pomat WS, van Haren SD, et al. (2019). Dynamic molecular changes during the first week of human life follow a robust developmental trajectory. Nat Commun 10, 1092. 10.1038/s41467-019-08794-x. [PubMed: 30862783]

24. Thome JJ, Bickham KL, Ohmura Y, Kubota M, Matsuoka N, Gordon C, Granot T, Griesemer A, Lerner H, Kato T, and Farber DL (2016). Early-life compartmentalization of human T cell differentiation and regulatory function in mucosal and lymphoid tissues. Nat Med 22, 72–77. 10.1038/nm.4008. [PubMed: 26657141]

25. Schreurs R, Baumdick ME, Sagebiel AF, Kaufmann M, Mokry M, Klarenbeek PL, Schaltenberg N, Steinert FL, van Rijn JM, Drewniak A, et al. (2019). Human Fetal TNF-alpha-Cytokine-Producing CD4(+) Effector Memory T Cells Promote Intestinal Development and Mediate Inflammation Early in Life. Immunity 50, 462–476 e468. 10.1016/j.immuni.2018.12.010. [PubMed: 30770246]

26. Schreurs R, Sagebiel AF, Steinert FL, Highton AJ, Klarenbeek PL, Drewniak A, Bakx R, The SML, Ribeiro CMS, Perez D, et al. (2021). Intestinal CD8(+) T cell responses are abundantly induced early in human development but show impaired cytotoxic effector capacities. Mucosal Immunol 14, 605–614. 10.1038/s41385-021-00382-x. [PubMed: 33772147]

27. Clark BL, and Thomas PG (2020). A Cell for the Ages: Human gammadelta T Cells across the Lifespan. Int J Mol Sci 21. 10.3390/ijms21238903.

28. Sallusto F, Langenkamp A, Geginat J, and Lanzavecchia A (2000). Functional subsets of memory T cells identified by CCR7 expression. Curr Top Microbiol Immunol 251, 167–171. [PubMed: 11036772]

29. Darrah PA, Patel DT, De Luca PM, Lindsay RW, Davey DF, Flynn BJ, Hoff ST, Andersen P, Reed SG, Morris SL, et al. (2007). Multifunctional TH1 cells define a correlate of vaccine-mediated protection against Leishmania major. Nat Med 13, 843–850. [PubMed: 17558415]

30. Schey R, Dornhoff H, Baier JL, Purtak M, Opoka R, Koller AK, Atreya R, Rau TT, Daniel C, Amann K, et al. (2016). CD101 inhibits the expansion of colitogenic T cells. Mucosal Immunol 9, 1205–1217. 10.1038/mi.2015.139. [PubMed: 26813346]

31. Shahin T, Kuehn HS, Shoeb MR, Gawriyski L, Giuliani S, Repiscak P, Hoeger B, Yuce Petronczki O, Bal SK, Zoghi S, et al. (2021). Germline biallelic mutation affecting the

transcription factor Helios causes pleiotropic defects of immunity. Sci Immunol 6, eabe3981. 10.1126/sciimmunol.abe3981.

32. Kim EY, Lynch L, Brennan PJ, Cohen NR, and Brenner MB (2015). The transcriptional programs of iNKT cells. Semin Immunol 27, 26–32. 10.1016/j.smim.2015.02.005. [PubMed: 25841627]
33. Hu G, and Chen J (2013). A genome-wide regulatory network identifies key transcription factors for memory CD8(+) T-cell development. Nat Commun 4, 2830. 10.1038/ncomms3830. [PubMed: 24335726]
34. Yoshitomi H, Kobayashi S, Miyagawa-Hayashino A, Okahata A, Doi K, Nishitani K, Murata K, Ito H, Tsuruyama T, Haga H, et al. (2018). Human Sox4 facilitates the development of CXCL13-producing helper T cells in inflammatory environments. Nat Commun 9, 3762. 10.1038/s41467-018-06187-0. [PubMed: 30232328]
35. Blom B, Heemskerk MH, Verschuren MC, van Dongen JJ, Stegmann AP, Bakker AQ, Couwenberg F, Res PC, and Spits H (1999). Disruption of alpha beta but not of gamma delta T cell development by overexpression of the helix-loop-helix protein Id3 in committed T cell progenitors. EMBO J 18, 2793–2802. 10.1093/emboj/18.10.2793. [PubMed: 10329625]
36. Kuo CT, and Leiden JM (1999). Transcriptional regulation of T lymphocyte development and function. Annu Rev Immunol 17, 149–187. [PubMed: 10358756]
37. Mackay LK, Minnich M, Kragten NA, Liao Y, Nota B, Seillet C, Zaid A, Man K, Preston S, Freestone D, et al. (2016). Hobit and Blimp1 instruct a universal transcriptional program of tissue residency in lymphocytes. Science 352, 459–463. 10.1126/science.aad2035. [PubMed: 27102484]
38. Kunkel EJ, Campbell JJ, Haraldsen G, Pan J, Boisvert J, Roberts AI, Ebert EC, Vierra MA, Goodman SB, Genovese MC, et al. (2000). Lymphocyte CC chemokine receptor 9 and epithelial thymus-expressed chemokine (TECK) expression distinguish the small intestinal immune compartment: Epithelial expression of tissue-specific chemokines as an organizing principle in regional immunity. J Exp Med 192, 761–768. [PubMed: 10974041]
39. Nakayamada S, Takahashi H, Kanno Y, and O'Shea JJ (2012). Helper T cell diversity and plasticity. Curr Opin Immunol 24, 297–302. 10.1016/j.coi.2012.01.014S0952-7915(12)00027-1 [pii]. [PubMed: 22341735]
40. Adkins B, Bu Y, and Guevara P (2001). The generation of Th memory in neonates versus adults: prolonged primary Th2 effector function and impaired development of Th1 memory effector function in murine neonates. J Immunol 166, 918–925. [PubMed: 11145668]
41. Adkins B, and Du RQ (1998). Newborn mice develop balanced Th1/Th2 primary effector responses in vivo but are biased to Th2 secondary responses. J Immunol 160, 4217–4224. [PubMed: 9574522]
42. Gibbons D, Fleming P, Virasami A, Michel ML, Sebire NJ, Costeloe K, Carr R, Klein N, and Hayday A (2014). Interleukin-8 (CXCL8) production is a signatory T cell effector function of human newborn infants. Nat Med 20, 1206–1210. 10.1038/nm.3670nm.3670 [pii]. [PubMed: 25242415]
43. Rivino L, Messi M, Jarrossay D, Lanzavecchia A, Sallusto F, and Geginat J (2004). Chemokine receptor expression identifies Pre-T helper (Th)1, Pre-Th2, and nonpolarized cells among human CD4+ central memory T cells. J Exp Med 200, 725–735. [PubMed: 15381728]
44. Singh SP, Zhang HH, Foley JF, Hedrick MN, and Farber JM (2008). Human T cells that are able to produce IL-17 express the chemokine receptor CCR6. J Immunol 180, 214–221. 180/1/214 [pii]. [PubMed: 18097022]
45. Miron M, Meng W, Rosenfeld AM, Dvorkin S, Poon MML, Lam N, Kumar BV, Louzoun Y, Luning Prak ET, and Farber DL (2021). Maintenance of the human memory T cell repertoire by subset and tissue site. Genome Med 13, 100. 10.1186/s13073-021-00918-7. [PubMed: 34127056]
46. Schenkel JM, Fraser KA, Beura LK, Pauken KE, Vezys V, and Masopust D (2014). T cell memory. Resident memory CD8 T cells trigger protective innate and adaptive immune responses. Science 346, 98–101. 10.1126/science.1254536science.1254536 [pii]. [PubMed: 25170049]
47. Rosato PC, Beura LK, and Masopust D (2017). Tissue resident memory T cells and viral immunity. Curr Opin Virol 22, 44–50. 10.1016/j.coviro.2016.11.011. [PubMed: 27987416]

48. Collins C, Sharpe E, Silber A, Kulke S, and Hsieh EWY (2021). Congenital Athymia: Genetic Etiologies, Clinical Manifestations, Diagnosis, and Treatment. J Clin Immunol 41, 881–895. 10.1007/s10875-021-01059-7. [PubMed: 33987750]
49. Cho JH, Boyman O, Kim HO, Hahm B, Rubinstein MP, Ramsey C, Kim DM, Surh CD, and Sprent J (2007). An intense form of homeostatic proliferation of naive CD8+ cells driven by IL-2. J Exp Med 204, 1787–1801. [PubMed: 17664294]
50. Kieper WC, Troy A, Burghardt JT, Ramsey C, Lee JY, Jiang HQ, Dummer W, Shen H, Cebra JJ, and Surh CD (2005). Recent immune status determines the source of antigens that drive homeostatic T cell expansion. J Immunol 174, 3158–3163. [PubMed: 15749843]
51. Purton JF, Tan JT, Rubinstein MP, Kim DM, Sprent J, and Surh CD (2007). Antiviral CD4+ memory T cells are IL-15 dependent. J Exp Med 204, 951–961. [PubMed: 17420265]
52. Pitt TJ, Becker AB, Chan-Yeung M, Chan ES, Watson WTA, Chooniedass R, and Azad MB (2018). Reduced risk of peanut sensitization following exposure through breast-feeding and early peanut introduction. J Allergy Clin Immunol 141, 620–625 e621. 10.1016/j.jaci.2017.06.024. [PubMed: 28916221]
53. Teijaro JR, Turner D, Pham Q, Wherry EJ, Lefrancois L, and Farber DL (2011). Cutting edge: tissue-retentive lung memory CD4 T cells mediate optimal protection to respiratory virus infection. J Immunol 187, 5510–5514. jimmunol.1102243 [pii]10.4049/jimmunol.1102243. [PubMed: 22058417]
54. Poon MML, Byington E, Meng W, Kubota M, Matsumoto R, Grifoni A, Weiskopf D, Dogra P, Lam N, Szabo PA, et al. (2021). Heterogeneity of human anti-viral immunity shaped by virus, tissue, age, and sex. Cell Rep 37, 110071. 10.1016/j.celrep.2021.110071. [PubMed: 34852222]
55. Torow N, Hand TW, and Hornef MW (2023). Programmed and environmental determinants driving neonatal mucosal immune development. Immunity 56, 485–499. 10.1016/j.immuni.2023.02.013. [PubMed: 36921575]
56. Weisberg SP, Ural BB, and Farber DL (2021). Tissue-specific immunity for a changing world. Cell 184, 1517–1529. 10.1016/j.cell.2021.01.042. [PubMed: 33740452]
57. Poon MML, Caron DP, Wang Z, Wells SB, Chen D, Meng W, Szabo PA, Lam N, Kubota M, Matsumoto R, et al. (2023). Tissue adaptation and clonal segregation of human memory T cells in barrier sites. Nat Immunol 24, 309–319. 10.1038/s41590-022-01395-9. [PubMed: 36658238]
58. Pugliese A, Yang M, Kusmarteva I, Heiple T, Vendrame F, Wasserfall C, Rowe P, Moraski JM, Ball S, Jebson L, et al. (2014). The Juvenile Diabetes Research Foundation Network for Pancreatic Organ Donors with Diabetes (nPOD) Program: goals, operational model and emerging findings. Pediatr Diabetes 15, 1–9. 10.1111/pedi.12097.
59. Sathaliyawala T, Kubota M, Yudanin N, Turner D, Camp P, Thome JJ, Bickham KL, Lerner H, Goldstein M, Sykes M, et al. (2013). Distribution and compartmentalization of human circulating and tissue-resident memory T cell subsets. Immunity 38, 187–197. 10.1016/j.immuni.2012.09.020S1074-7613(12)00521-3 [pii]. [PubMed: 23260195]
60. Carpenter DJ, Granot T, Matsuoka N, Senda T, Kumar BV, Thome JJC, Gordon CL, Miron M, Weiner J, Connors T, et al. (2018). Human immunology studies using organ donors: Impact of clinical variations on immune parameters in tissues and circulation. Am J Transplant 18, 74–88. 10.1111/ajt.14434. [PubMed: 28719147]
61. Granot T, Senda T, Carpenter DJ, Matsuoka N, Weiner J, Gordon CL, Miron M, Kumar BV, Griesemer A, Ho SH, et al. (2017). Dendritic Cells Display Subset and Tissue-Specific Maturation Dynamics over Human Life. Immunity 46, 504–515. 10.1016/j.immuni.2017.02.019. [PubMed: 28329707]
62. Love MI, Huber W, and Anders S (2014). Moderated estimation of fold change and dispersion for RNA-seq data with DESeq2. Genome Biol 15, 550. 10.1186/s13059-014-0550-8. [PubMed: 25516281]
63. Hulsen T, de Vlieg J, and Alkema W (2008). BioVenn - a web application for the comparison and visualization of biological lists using area-proportional Venn diagrams. BMC Genomics 9, 488. 10.1186/1471-2164-9-488. [PubMed: 18925949]
64. Kolde R (2012). Pheatmap: pretty heatmaps. R package version 1.

65. Mootha VK, Lindgren CM, Eriksson KF, Subramanian A, Sihag S, Lehar J, Puigserver P, Carlsson E, Ridderstrale M, Laurila E, et al. (2003). PGC-1alpha-responsive genes involved in oxidative phosphorylation are coordinately downregulated in human diabetes. Nat Genet 34, 267–273. 10.1038/ng1180. [PubMed: 12808457]

66. Subramanian A, Tamayo P, Mootha VK, Mukherjee S, Ebert BL, Gillette MA, Paulovich A, Pomeroy SL, Golub TR, Lander ES, and Mesirov JP (2005). Gene set enrichment analysis: a knowledge-based approach for interpreting genome-wide expression profiles. Proc Natl Acad Sci U S A 102, 15545–15550. 10.1073/pnas.0506580102. [PubMed: 16199517]

67. Bolotin DA, Poslavsky S, Mitrophanov I, Shugay M, Mamedov IZ, Putintseva EV, and Chudakov DM (2015). MiXCR: software for comprehensive adaptive immunity profiling. Nat Methods 12, 380–381. 10.1038/nmeth.3364. [PubMed: 25924071]

68. DeWolf S, Grinshpun B, Savage T, Lau SP, Obradovic A, Shonts B, Yang S, Morris H, Zuber J, Winchester R, et al. (2018). Quantifying size and diversity of the human T cell alloresponse. JCI Insight 3. 10.1172/jci.insight.121256.

69. Virtanen P, Gommers R, Oliphant TE, Haberland M, Reddy T, Cournapeau D, Burovski E, Peterson P, Weckesser W, Bright J, et al. (2020). SciPy 1.0: fundamental algorithms for scientific computing in Python. Nat Methods 17, 261–272. 10.1038/s41592-019-0686-2. [PubMed: 32015543]

Highlights

- Memory T cells preferentially accumulate in human mucosal tissues during early life.
- Tissue resident memory T cells (TRM) undergo functional maturation over childhood
- TRM exhibit distinct transcriptional programs and site-specific expansion over age.

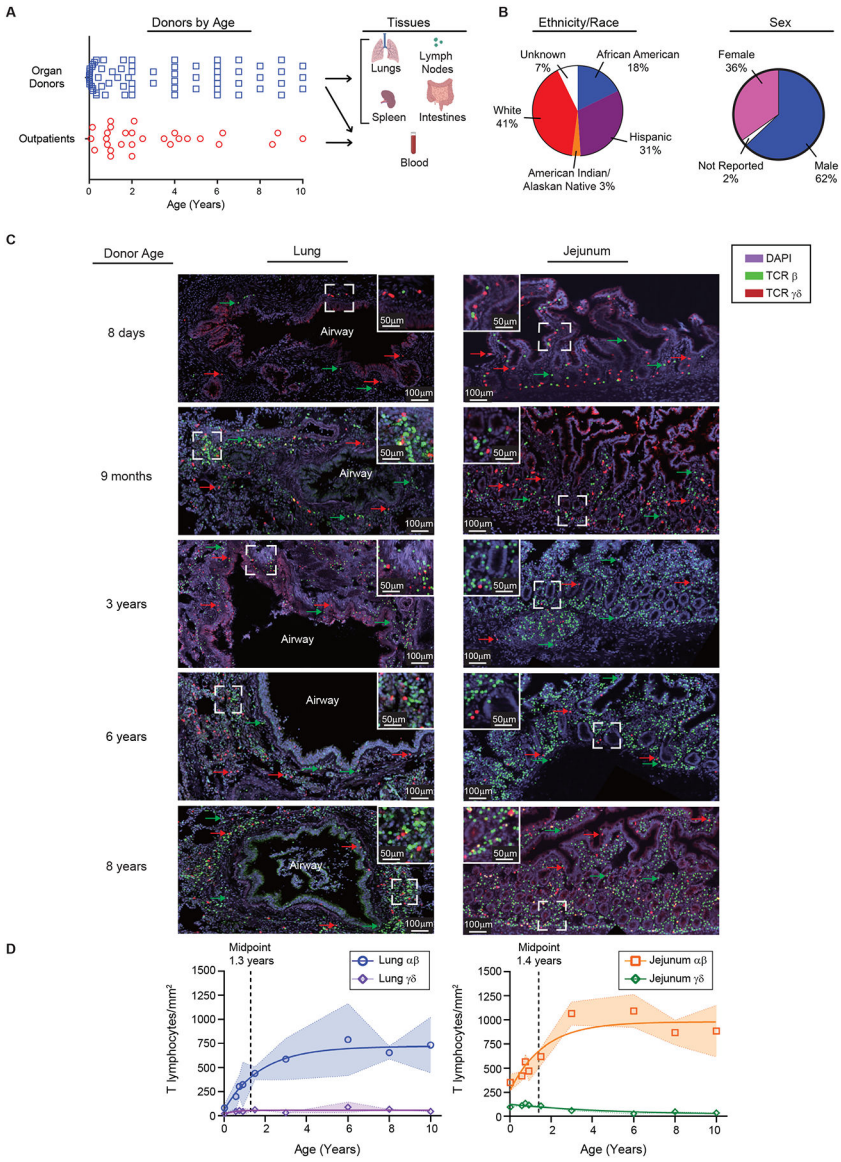

Figure 1. Pediatric samples for examining T cell differentiation across blood and tissues over childhood and accumulation in mucosal sites.

(A) Donor and subjects included in this study organized by age (left; organ donors: n=68, outpatients: n=28) and samples (right) used in this study. (B) Donor and subject demographics. Pie charts show stratification of pediatric donors and subjects combined by reported ethnicity and race. (C) T cell accumulation in mucosal sites over early life and childhood. Immunofluorescence imaging on sections obtained from lungs and intestines of organ donors (n=9). Representative staining with antibodies to T cell receptor (TCR) β, TCR γδ, and DAPI on lung (left) and jejunum (right) sections from 5 organ donors paired by row. $CD3^+$ cells are shown based on their expression of TCR β (green) and TCR γδ (red). Sections shown at 40x magnification (with line demonstrating 100μm distance) with dotted square box shown as inset at 80x (line depicting 50μm distance). (D) Compiled analysis of αβ and γδ T cells by area (y-axis, cells/mm^2) and age (x-axis, years) from lung (left) and jejunum (right). Data points represent mean cell/mm^2 of sections from each

individual donor (n=3–6 sections/donor) with shading depicting one standard deviation from the mean. Statistical testing was performed by Pearson correlation demonstrated correlation between age and cells/mm^2: lung αβ; p=0.0025, jejunum αβ; p = 0.0292, and jejunum γδ; p = 0.0026. Line depicts best fit as determined by modeling (see methods). T cell subsets displayed as lung αβ (blue circles), lung γδ (purple diamonds), jejunum αβ (orange squares), jejunum γδ (green diamonds). See also Figures S1–3 and Table S1.

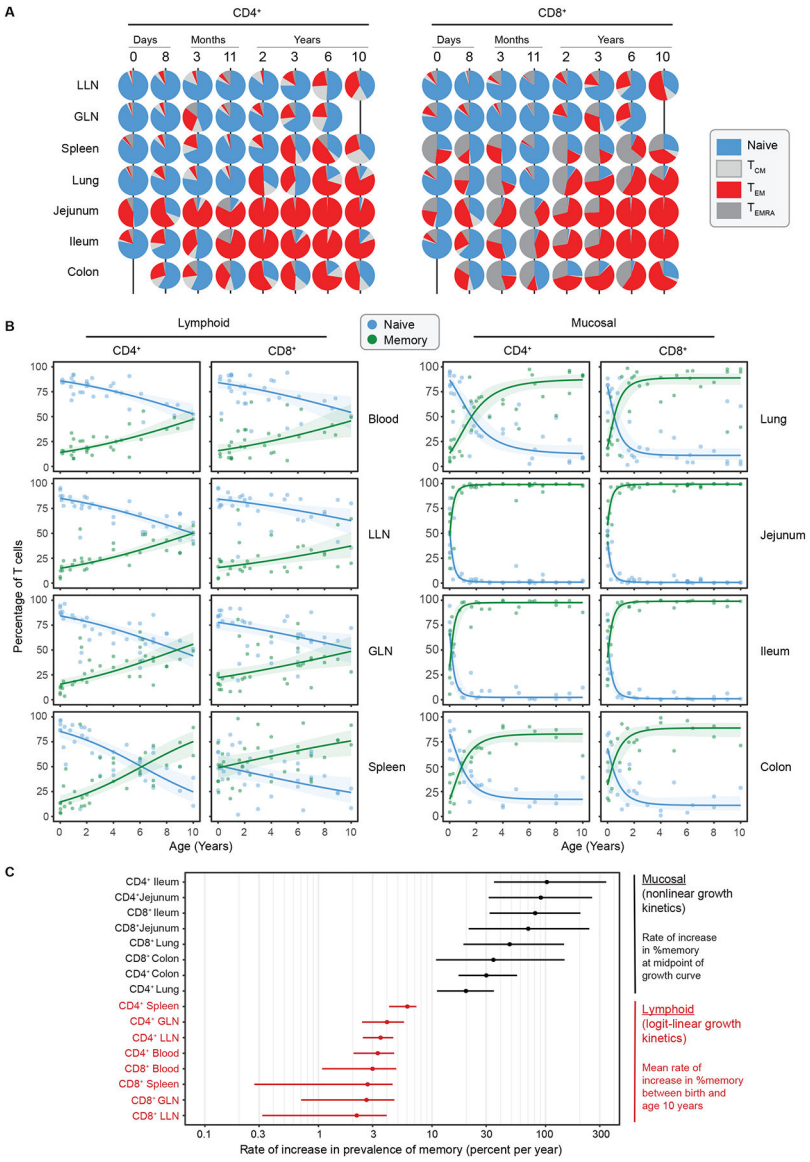

Figure 2. Memory T cells develop rapidly in mucosal sites with slower accumulation in blood and lymphoid organs.

High-dimensional flow cytometry analysis was performed to identify major T cell subsets by tissue and age. (A) T cell subsets were defined by expression of CCR7 and CD45RA: Naïve ($CCR7^+CD45RA^+$, blue), Central Memory (T_{CM} cells; $CCR7^+CD45RA^-$, light gray), Effector Memory (T_{EM} cells; $CCR7^-CD45RA^-$, red), and Effector Memory cells expressing CD45RA (T_{EMRA} cells; $CCR7^-CD45RA^+$, dark gray). Piecharts showing the proportion of $CD4^+$ (left) and $CD8^+$ (right) memory subsets within each tissue (row) for representative donors (column) of indicated ages over the first 10 years of life. (B) Compiled data from all donors showing relationship of total memory cells (T_{EM} + T_{CM} + T_{EMRA}) (green) to naïve (blue) T cells vs age over the first 10 years of life, organized by tissue with lymphoid (left; blood n = 31, spleen n = 36, lung lymph node (LLN) n = 33, gut lymph node (GLN) n = 35) and mucosal (right; lung n = 36, jejunum n = 41, ileum n = 29, and colon n= 25). Lines depict best fitting model (see methods) logit-linear (lymphoid tissues) or nonlinear

(mucosal tissues) with shading indicating 95% confidence intervals. C) Graph depicts log scaled maximal % accumulation rate per year (x-axis) of $CD4^+$ and $CD8^+$ memory T cells by tissue site (y-axis) with data organized by highest to lowest rate. Dots represent mean and bars represent 95% confidence intervals. See also Figure S2–5 and Table S1.

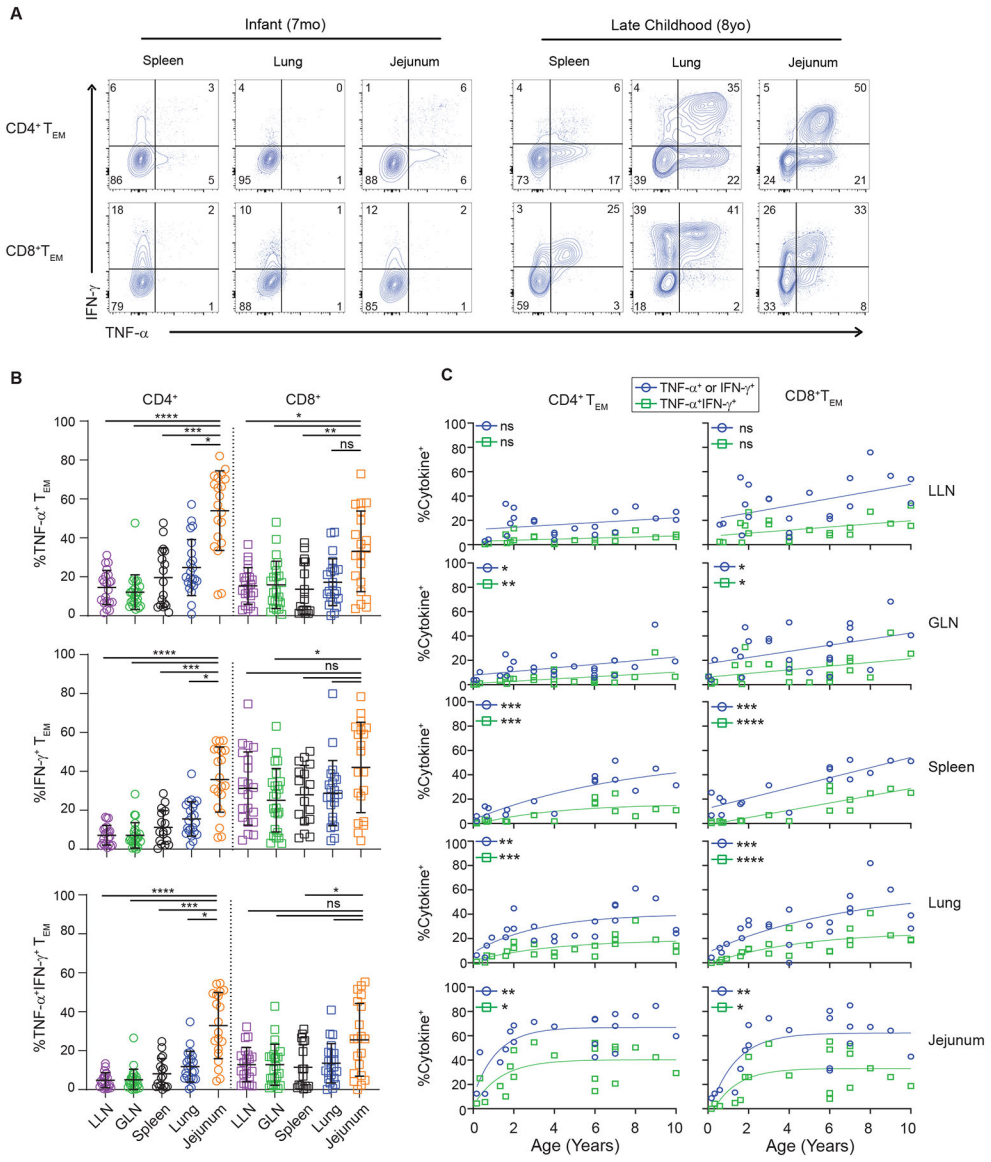

Figure 3. Functional maturation of effector-memory T cells over childhood.

T cells from lymphoid and mucosal sites of organ donors aged 0–10 years were stimulated with PMA/ionomycin and effector cytokine production (TNF-α, IFN-γ) from T_{EM} cells was assessed by intracellular cytokine staining (ICS). (A) Representative cytokine production by $CD4^+$ (top) and $CD8^+$ (bottom) T_{EM} cells from indicated tissues obtained from an infant (7 months, left) and older pediatric (8 years, right) organ donor, showing frequency of IFN-γ^+, TNF-α^+ or IFN-γ/TNF-α^+ cells in each site. Quadrants delineated based on unstimulated controls. (B) Effector cytokine production stratified by tissue site. Plots show cytokine production (TNFα^+ (top), IFNγ^+ (middle), and TNFα^+/IFNγ^+ (bottom)) by $CD4^+$ (left) and $CD8^+$ (right) T_{EM} cells for each site for each individual pediatric donor. Lines depict mean with standard deviation. Statistical testing by Kruskal-Wallis Anova with Dunn's correction for multiple comparisons. (C) Progressive acquisition of effector function over childhood. Cytokine production by $CD4^+$ (left) and $CD8^+$ (right) T_{EM} cells in indicated sites over age

showing frequency of cells expressing either TNFα$^+$ or IFNγ$^+$ (blue circles) and or both TNFα$^+$/IFNγ$^+$ (green squares). Lines depict best fitting linear or nonlinear model. Statistical testing using Spearman correlation. Donors; lung lymph node n= 21, gut lymph node n = 24, spleen n = 17, lung n = 22, and jejunum n=20. ns = p>0.05, * = p<0.05, **= p<0.01, ***=p<0.001, ****=p<0.0001. See also Figures S2,S6 and Table S1.

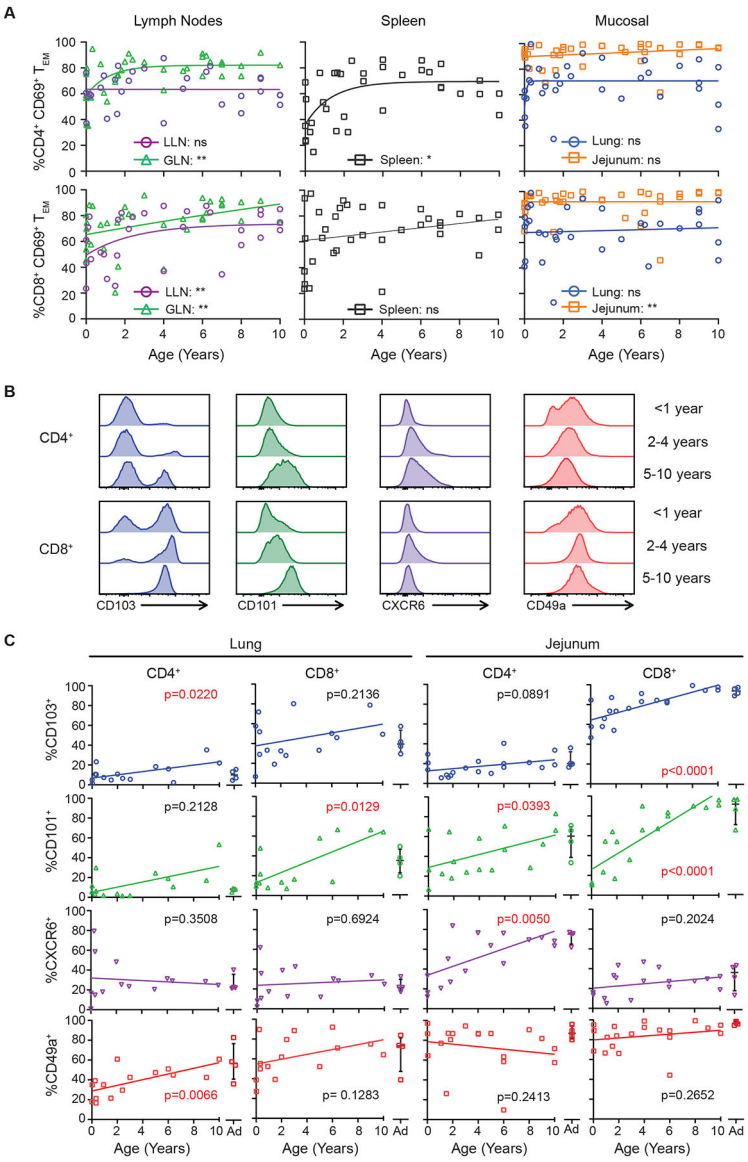

Figure 4. Site- and age-regulated expression of tissue resident markers by mucosal memory T cells.

Flow cytometric analysis of expression of CD69 on effector memory (T_{EM}) T cells. (A) Compiled data of all $CD4^+$ (top) and $CD8^+$ (bottom) % $CD69^+$ T_{EM} cells over age based on tissue site. Data organized by left (lymph nodes (LN); lung, gut), middle (spleen), right (mucosal; lung and jejunum). Statistical testing via Pearson or Spearman correlation with lines depicting best fitting model (linear vs nonlinear). Donors; spleen n = 35, LLN n = 31, GLN n = 36, lung n = 33, jejunum n = 39. (B) Flow cytometry histograms of core T_{RM} marker expression by $CD4^+$ (top) and $CD8^+$ (bottom) $CD69^{hi}$ T_{EM} cells from the jejunum of representative donors displayed by age grouping; <1 year, 2–4 years, and 5–10 years. Histograms normalized to mode. (C) Expression of T_{RM} cell core markers (CD103, CD101, CXCR6, and CD49a) in the lung and jejunum over age shown in compiled data from infant (n=13–16) and adult organ donors (n=4 per graph, 8 total donors) by $CD4^+$ (left) and $CD8^+$ (right) $CD69^+$ T_{EM} cells. Values from adult donors (aged 20–50 years) are shown in each

plot. Statistical testing performed using Pearson or Spearman correlation. * = $p<0.05$, ** $p<0.01$. See also Figures S2,S7 and Tables S1.

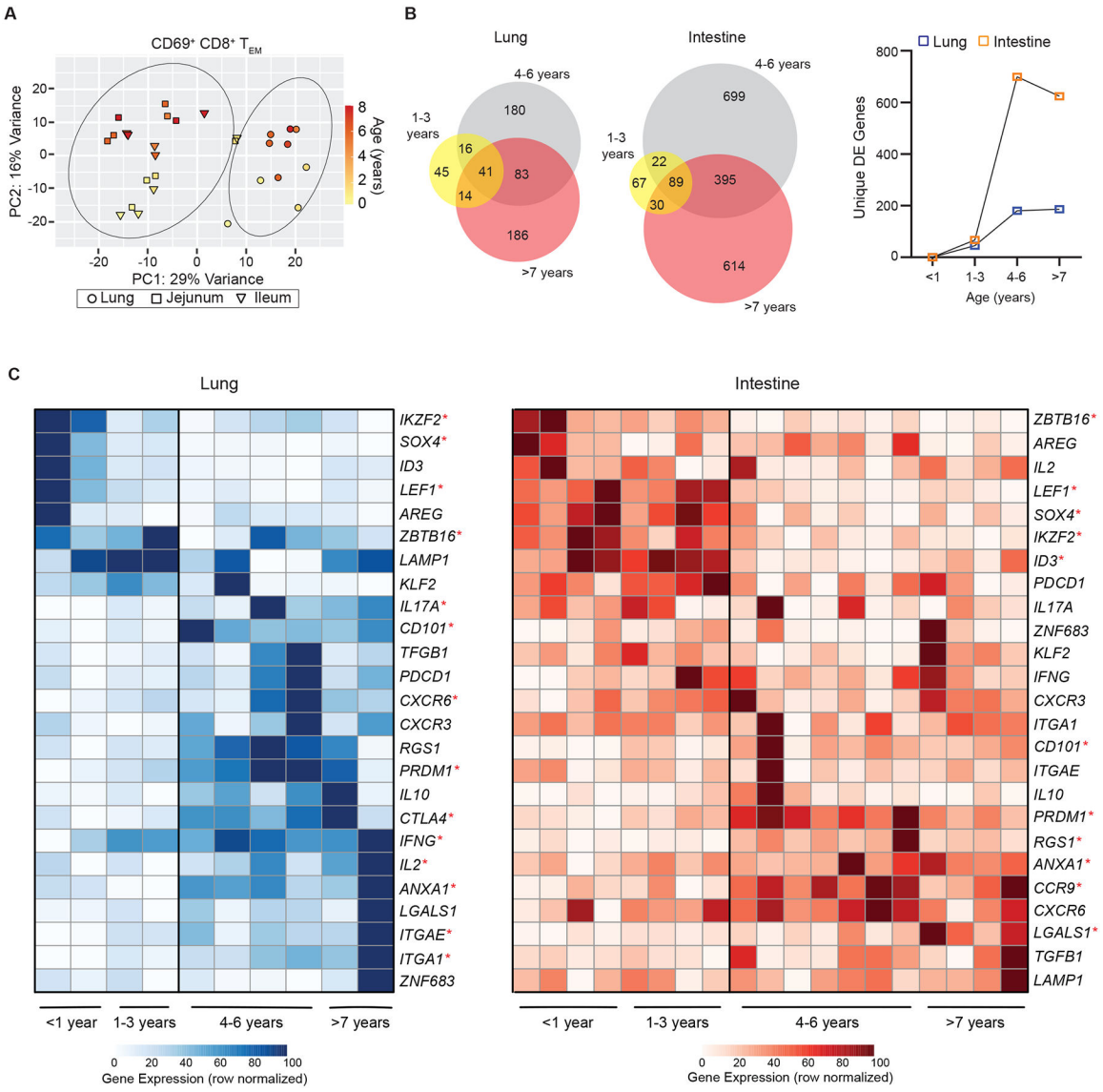

Figure 5. Transcriptional maturation of mucosal memory T cells over childhood.

$CD8^+CD69^+T_{EM}$ cells were sorted from lungs and intestines from donors of indicated ages for whole transcriptome profiling by RNAseq (See methods). (A) Principal component analysis (PCA) of samples from the lung (circles; n = 10) and intestine squares; jejunum n=10, and triangle; ileum n=9) from n=11 organ donors (aged 3 months – 8 years) colored based on donor age. Circles represent one standard deviation based on tissue site (lung or intestine). (B) Differentially expressed (DE) genes from pediatric organ donors based on age groups (1–3 years, 4–6 years, and >7 years) relative to the youngest donors (<1 year). Venn diagrams (left) depicting DE genes (log2fold > ±0.5, p<0.05) within and across donor groups compared to the youngest donors. Line graph depicting unique DE genes in each age group compared to youngest donor group (lungs; blue squares and intestines; orange squares). (C) Heatmaps depicting row normalized gene expression of key genes differentially expressed over age by memory T cells isolated from lungs (left) and intestines

(right) with donors (columns) arranged in increasing age. Statistical testing by Spearman or Pearson correlation analysis. * = $p<0.05$. See also Figure S2,S8 and Table S1–4.

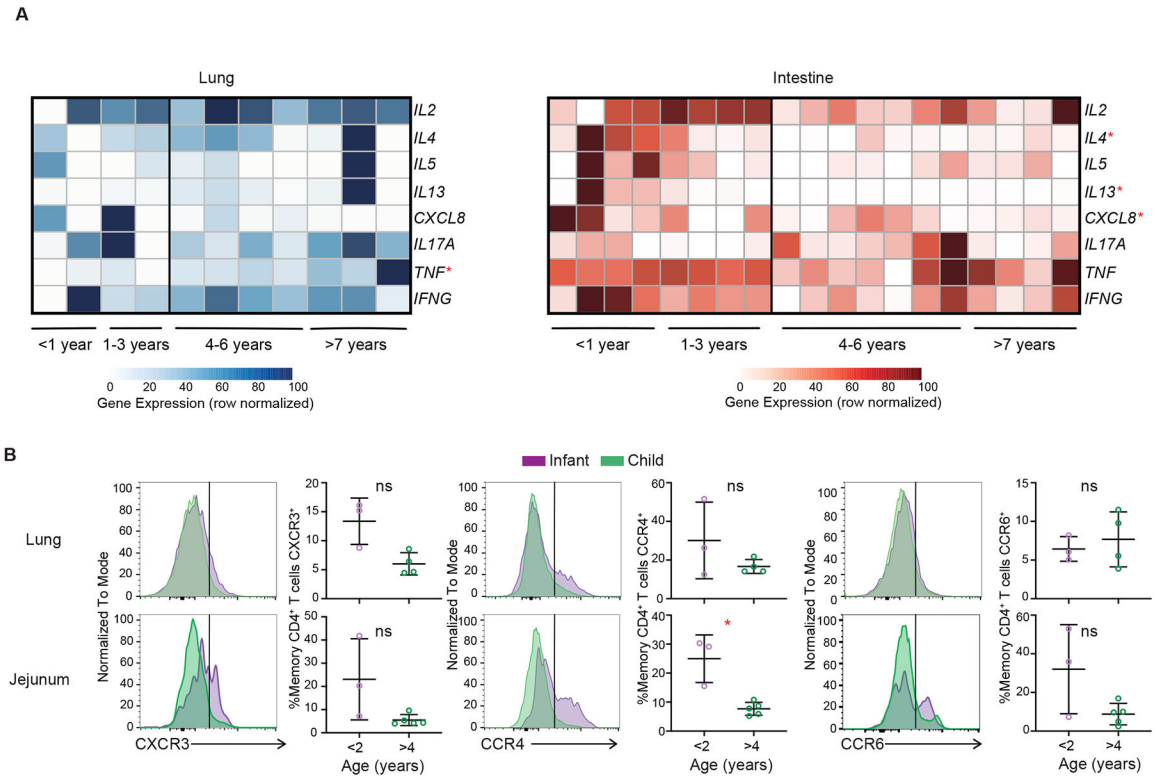

Figure 6: Dynamic shifts in functional capacity for memory CD4$^+$ T cells over childhood.

(A) Heatmaps depicting row normalized cytokine gene expression from CD69$^+$ CD4$^+$ T_{EM} cells within mucosal sites (lung; blue circles, n = 10 and intestine (jejunum and ileum); orange squares, n = 19) from n = 11 organ donors over age (0.3 – 8 years)). Statistical testing by Pearson or Spearman correlation. (B) Expression of indicated chemokine receptors denoting T-helper cell differentiation states by memory CD4$^+$ T cells in lung (top; n=7) and jejunum (bottom; n=8) from organs donors aged 0.02–7 years shown as representative histograms (normalized to mode) from infant (<2 years; purple) and older child (>4 years; green) and compiled data from multiple donors. Statistical testing done with Mann-Whitney T test, lines depict mean and standard deviation. * = p <0.05, ** = p <0.01, *** = p<0.001. LLN = lung lymph node, GLN = gut lymph node. See also Figure S2 and Tables S1,S2.

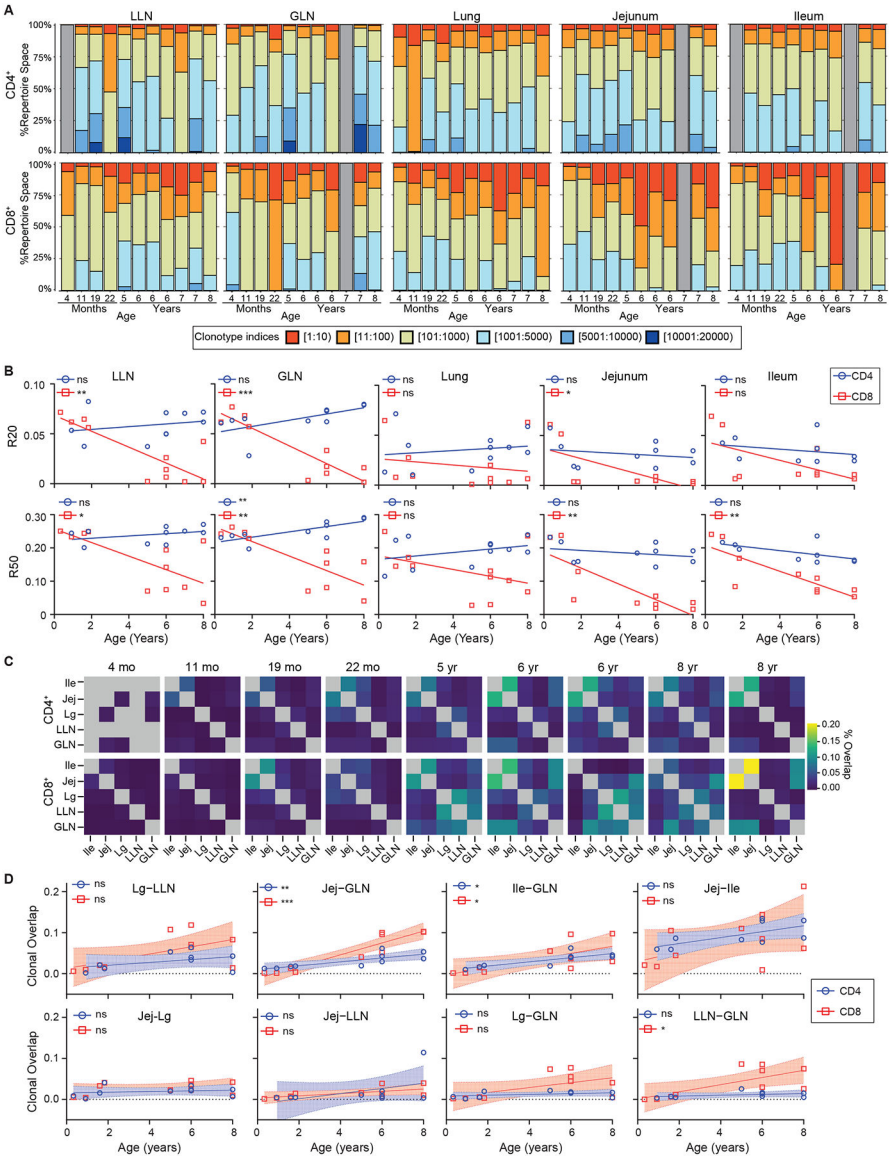

Figure 7. T cell receptor analysis reveals loss of diversity and differential overlap between sites over age.

T cell receptor (TCR) analysis performed on population RNA sequencing of CD69$^+$ T_{EM} cells as in Fig. 5. (A) Clonotype analysis organized by tissue site (columns) and CD4$^+$ (top) and CD8$^+$ (bottom) with proportion of repertoire space (y-axis) occupied by clonotypes vs individual donors (x-axis; stacks) organized by increasing age. Gray bars depict donors/tissues were no sample was available. (B) R20 (top) and R50 (bottom) over age for CD4$^+$ (blue circles) and CD8$^+$ (red squares) T cells by tissue site. Statistical testing performed by Wald test. Line depicts best fitting linear or non-linear model. (C) Clonal overlap matrices for individual donors with CD4$^+$ (top) and CD8$^+$ (bottom) organized by individual donors (columns) by increasing age. Box color depicts % overlap. Gray boxes depict tissues were no sample was available. (D) Dotplots showing clonal overlap over age (years) for CD4$^+$ (blue circles) and CD8$^+$ (red squares) T cells. Line depicts best fit with 95% confidence

interval. Statistical testing with Wald test. ns = $p>0.05$, * = $p<0.05$, ** = $p<0.01$, *** = $p<0.001$, **** = $p<0.0001$.

Abbreviations; Ile- Ileum, Jej- Jejunum, Lg- Lung. See also Tables S1,S5.

KEY RESOURCES TABLE

Reagent or Resource	Source	Identifier
Antibodies		
Flow Cytometry		
Anti-Human CCR4 BV605	Biolegend	L291H4, Cat. #359418
Anti-Human CCR6 BV480	BD Biosciences	11A9, Cat. #11A9
Anti-Human CD101 APC	Biolegend	BB27; Cat. # 331007
Anti-Human CD101 BV786	BD Biosciences	V7.1; Cat. # 747545
Anti-Human CD103 BB515	BD Biosciences	Ber-ACT8; Cat 564578
Anti-Human CD103 BUV395	BD Biosciences	Ber-ACT8; Cat. # 564346
Anti-Human CD103 PE/Cy7	Biolegend	Ber-ACT8; Cat. # 350212
Anti-Human CD103 PerCP/Cy.5.5	Biolegend	Ber-ACT8; Cat. # 350226
Anti-Human CD127 AF647	Biolegend	A019D5; Cat. # 351318
Anti-Human CD127 APC-R700	BD Biosciences	HIL-7R-M21; Cat. #565185
Anti-Human CD127 BV510	Biolegend	A019D5; Cat. # 351332
Anti-Human CD197 (CCR7) AF488	Biolegend	G043H7; Cat. # 353206
Anti-Human CD197 (CCR7) BV650	Biolegend	G043H7; Cat. # 353234
Anti-Human CD25 APC	Biolegend	BC96; Cat. # 302610
Anti-Human CD25 BV605	Biolegend	BC96; Cat. # 302632
Anti-Human CD25 PE	Biolegend	BC96; Cat. # 302606
Anti-Human CD279 (PD-1) BB700	BD Biosciences	EH12.1; Cat. # 566460
Anti-Human CD3 BV510	Biolegend	OKT3; Cat. # 317332
Anti-Human CD3 BV605	Biolegend	OKT3; Cat. # 317322
Anti-Human CD3 BV650	Biolegend	OKT3; Cat. # 317324
Anti-Human CD4 BU737	BD Biosciences	SK3; Cat. # 612748
Anti-Human CD4 BV421	Biolegend	SK3; Cat. # 344632
Anti-Human CD4 PE/Cy7	Biolegend	SK3; Cat. # 980808
Anti-Human CD4 cFluor YG584	Cytek	SK3; Cat. #R7-20041
Anti-Human CD45 Alexa Fluor® 700	Biolegend	2D1; Cat. # 368514
Anti-Human CD45 PerCP	Biolegend	HI30; Cat. #304026
Anti-Human CD45RA BV570	Biolegend	HI100; Cat. 304132
Anti-Human CD45RA BV605	Biolegend	HI100; Cat. # 304134
Anti-Human CD45RA PE/Cy7	Biolegend	HI100; Cat. # 304126
Anti-Human CD45RA PerCP/Cy.5.5	Biolegend	HI100; Cat. # 304122
Anti-Human CD45RO PerCP/Cy.5.5	Biolegend	UCHL1; Cat. # 304222
Anti-Human CD45RO PerCP-eFluor710	eBioscience	UCHL1; Cat. # 46-0457-42
Anti-Human CD49a BUV615	BD Biosciences	SR84; Cat. # 751437
Anti-Human CD49a PE	Biolegend	TS2/7; Cat. # 328304
Anti-Human CD69 BV711	Biolegend	FN50; Cat. # 310944

Reagent or Resource	Source	Identifier
Anti-Human CD69 PE/Dazzle 594	Biolegend	FN50; Cat. # 310942
Anti-Human CD69 PerCP/Cy.5.5	Biolegend	FN50; Cat. # 310926
Anti-Human CD8 APC/Fire 750	Biolegend	SK1; Cat. # 344746
Anti-Human CD8 BUV496	BD Biosciences	RPA-T8; Cat. # 612942
Anti-Human CD8 BV711	Biolegend	SK1; Cat. # 344734
Anti-Human CD8 BV805	BD Biosciences	SK1; Cat. # 612889
Anti-Human CXCR3 BB700	BD Biosciences	1C6/CXCR3, Cat. # 566532
Anti-Human CXCR6 BV750	BD Biosciences	13B 1E5; Cat. # 747052
Anti-Human CXCR6 PE/Dazzle 594	Biolegend	K041E5; Cat. # 356016
Anti-Human FoxP3 PE	Invitrogen	236A/E7; Cat. # 72-5774-40
Anti-Human FoxP3 PE/Dazzle 594	Biolegend	206D; Cat. # 320126
Anti-Human IFNγ BV480	BD Biosciences	B27, Cat. #566100
Anti-Human TCR γ/δ PerCP-eFlour710	Invitrogen	B1.1; Cat. #46-9959-42
Anti-Human TCR γ/δ BV421	Biolegend	B1; Cat. # 331217
Anti-Human TNFα BV785	Biolegend	Mab11; Cat. #502948
Biological Samples		
Human Pediatric deceased Organ Donor samples	Organ procurement organizations throughout the USA	https://bruskolab.diabetes.ufl.edu/research/handel-i/
Human adult deceased organ donor samples	LiveOnNY	https://www.liveonny.org/
Human Subjects Blood Samples	NYP Audubon Clinic	CUIMC IRB #AAAQ6732
Immunofluorescence Imaging		
Anti-Hu TCR V beta F1 APC	Invitrogen	8A3; Cat. # 17-5766-42
Anti-Hu TCR $\gamma\delta$ PE	Life Technologies	MHGD04; Cat. # 2188772
Anti-Hu CD3 Alexa Flour488	Biolegend	OKT3; Cat. # 317310
Chemicals, peptides and recombinant proteins		
10% Zinc Formalin	Anatech	Cat # 170
ACK Lysing buffer	Gibco	Ref#A10492-01
β-mercaptoethanol	Sigma	Cat#M6350-250ML
Collagenase	Millipore Sigma	Cat#11088882001
DAPI	Chemometec	Cat. # 910-3013
DNAse	Millipore Sigma	Cat#DN25-5G
DPBS	Corning	Cat #20-030-CV
EDTA	Corning	Cat #46-034-CI
Fetal Bovine Serum	GeminiBio	Cat#100-106
Fixable Viability Dye eFIuor™ 780	Thermo Fisher Scientific	Cat. # 65-0865-18
Fixable Viability Dye Zombie NIR	Biolegend	Cat. # 423106
Fixation Buffer	Invitrogen	Cat#00-5223-56
GolgiPlug	BD Biosciences	Cat#555029

Reagent or Resource	Source	Identifier
GolgiStop	BD Biosciences	Cat#554724
IMDM	Gibco	Ref#122440-053
Ionomycin	Sigma	Cat#I9657
Lymphocyte Separation Media	Corning	Cat#25-072-CI
O.C.T. Compound	Fisher Healthcare	Cat#23-730-571
Penicillin/Streptomycin/L-glutamine	GeminiBio	Cat#c400-110
Permeabilization Buffer	Invitrogen	Cat#00-8333-56
PMA	Sigma	Cat#P1585
RLT Buffer	Qiagen	Cat#1053393
Rneasy Micro Kit	Qiagen	Cat#74004
RPMI 1640	Corning	Cat #10-040-CM
TrueStain FcX	BioLegend	Cat #422302
True-Stain Monocyte Blocker	BioLegend	Cat #426102
Critical Commercial Assays		
RNA 6000 Pico Kit	Agilent	Cat#5067-1513
SMART-Seq Ultra-low input RNA kit	Takara Bio	Cat#634894
Deposited Data		
Population RNA-seq Data	This article	GSE220094
Software and Algorithms		
Imaris Software v9.8.2	Oxford Instruments	https://imaris.oxinst.com
FlowJo v 10.7 software	Tree Start	https://www.flowjo.com
FCS express v 7.12.0005 software	Denovo Software	https://denovosoftware.com
GSEA v4.3.1	UC San Diego/ Broad Institute	https://www.gsea-msigdb.org/gsea/index.isp
Prism v 9.4.0 software	GraphPad	www.graphpad.com
Rstudio version	Rstudio, Inc. (2019)	https://www.rstudio.com
R version	R Foundation for Statistical Computing	https://www.R-project.com